Investigating stable oxygen and carbon isotopic variability in speleothem records over the last millennium using multiple isotope-enabled climate models

Janica C. Bühler[1]⋆, Josefine Axelsson[2]⋆, Franziska A. Lechleitner[3], Jens Fohlmeister[4,5], Allegra N. LeGrande[6], Madhavan Midhun[7,8], Jesper Sjolte[9], Martin Werner[10], Kei Yoshimura[11], and Kira Rehfeld[1,12]

[1]Institute of Environmental Physics, Heidelberg University, D-69120 Heidelberg, Germany
[2]Department of Physical Geography and Bolin Centre for Climate Research, Stockholm University, SE-106 91 Stockholm, Sweden
[3]Department of Chemistry, Biochemistry and Pharmaceutical Sciences and Oeschger Centre for Climate Change Research, University of Bern, 3012 Bern, Switzerland
[4]Federal Office for Radiation Protection, D-10318 Berlin, Germany
[5]GFZ German Research Centre for Geosciences, Section "Climate Dynamics and Landscape Development", D-14473 Potsdam, Germany
[6]NASA Goddard Institute for Space Studies and Center for Climate Systems Research, Columbia University, New York, USA
[7]Department of Atmospheric Sciences, Cochin University of Science and Technology, India
[8]Earth Research Institute, University of California Santa Barbara, CA, USA
[9]Department of Geology, Lund University, SE-223 62 Lund, Sweden
[10]Alfred Wegener Institute, Helmholtz-Centre for Polar and Marine Research, D-27515 Bremerhaven, Germany
[11]Institute of Industrial Science, The University of Tokyo, 5-1-5, Kashiwanoha, Kashiwa-shi, Chiba, 277-8574, Japan
[12]Department of Geoscience, Geo- und Umweltforschungszentrum, Schnarrenbergstr. 94-96, D-72074 Tübingen, Germany

⋆These authors contributed equally to this work
Correspondence to: J. C. Bühler (jbuehler@iup.uni-heidelberg.de) and J. Axelsson (josefine.axelsson@natgeo.su.se)

Abstract. The incorporation of water isotopologues into the hydrology of general circulation models (GCMs) facilitates the comparison between modelled and measured proxy data in paleoclimate archives. However, the variability and drivers of measured and modelled water isotopologues, and indeed the diversity of their representation in different models are not well constrained. Improving our understanding of this variability in past and present climates will help to better constrain future

5 climate change projections and decrease their range of uncertainty. Speleothems are a precisely datable terrestrial paleoclimate archive and provide well preserved (semi-)continuous multivariate isotope time series in the lower and mid-latitudes, and are, therefore, well suited to assess climate and isotope variability on decadal and longer timescales. However, the relationship between speleothem oxygen and carbon isotopes to climate variables are influenced by site-specific parameters, and their comparison to GCMs is not always straightforward.

10 Here we compare speleothem oxygen and carbon isotopic signatures from the Speleothem Isotopes Synthesis and AnaLysis database version 2 (SISALv2) to the output of five different water-isotope-enabled GCMs (ECHAM5-wiso, GISS-E2-R, iCESM, iHadCM3, and isoGSM) over the last millennium (850–1850 common era, CE). We systematically evaluate differences and commonalities between the standardized model simulation outputs. The goal is to distinguish climatic drivers of variability for modelled isotopes and compare them to those of measured isotopes.

15 We find strong regional differences in the oxygen isotope signatures between models that can partly be attributed to differences in modelled surface temperature. At low latitudes, precipitation amount is the dominant driver for stable water isotope variability, however, at cave locations the agreement between modelled temperature variability is higher than for precipitation variability. While modelled isotopic signatures at cave locations exhibited extreme events coinciding with changes in volcanic and solar forcing, such fingerprints are not apparent in the speleothem isotopes. This may be attributed to the lower

temporal resolution of speleothem records compared to the events that are to be detected. Using spectral analysis, we can show that all models underestimate decadal and longer variability compared to speleothems, although to varying extent.

We found that no model excels in all analyzed comparisons, although some perform better than the others in either mean or variability. Therefore, we advise a multi-model approach, whenever comparing proxy data to modelled data. Considering karst and cave internal processes through e.g. isotope-enabled karst models may alter the variability in speleothem isotopes and play an important role in determining the most appropriate model. By exploring new ways of analyzing the relationship between the oxygen and carbon isotopes, their variability, and co-variability across timescales, we provide methods that may serve as a baseline for future studies with different models using e.g. different isotopes, different climate archives, or time periods.

1 Introduction

Under the current anthropogenic warming trend (Shukla et al., 2019), the interest in understanding its impacts on the mean temperature and precipitation and changes in their variability increases. Evaluating the representation of the mean state as well as variability of past climate as simulated by climate models is crucial for reliable future projections (Schmidt et al., 2012). The abundance of the heavy oxygen isotope ^{18}O to ^{16}O in stable water isotopologues (SWI), further denoted as $\delta^{18}O$, is a proxy and tracer of natural variability in the water cycle. Oxygen isotope compositions can be measured in many paleoclimate proxy archives such as trees, ice cores, corals, or marine and lake sediments, which collectively extend our knowledge of climatic changes beyond the instrumental record (Bradley, 1999). Speleothems are secondary cave carbonate deposits, which form in karst systems globally, most commonly in the low- to mid-latitudes, under a wide range of climate conditions Fairchild and Baker (2012). They provide precisely and absolutely dated, (semi-)continuous time series of proxy data (Comas-Bru et al., 2019), and have long been used as archives for terrestrial climate (Hendy, 1971). Oxygen isotopes are incorporated in calcite or aragonite matrices in accumulated growth layers. The stable carbon isotopic ratio ($\delta^{13}C$) is a second useful proxy for climate and vegetation conditions (Wong and Breecker, 2015).

Broad correspondence between speleothem $\delta^{18}O$ and surface temperature (e.g. McDermott et al., 2001) or local rainfall strength and seasonality (e.g. Medina-Elizalde et al., 2016; Kennett et al., 2012; Cheng et al., 2016), and between speleothem $\delta^{13}C$ and vegetation cover can be resolved in regional and global analyses (Comas-Bru et al., 2019; Fohlmeister et al., 2020; Baker et al., 2019; Lechleitner et al., 2021). Modification of these signatures by vadose-zone fractionation processes (Tremaine et al., 2011; Grossman and Ku, 1986; Romanek et al., 1992), karst hydrology, and internal cave conditions (Fairchild and Baker, 2012; Wackerbarth et al., 2010; Jean-Baptiste et al., 2019; Fohlmeister et al., 2020), and differences in geochronological methods between records can complicate paleoclimatic interpretations (Breitenbach et al., 2012; Rehfeld and Kurths, 2014). Age-model standardization (Comas-Bru et al., 2020b), multiproxy approaches (Tremaine and Froelich, 2013; Warken et al., 2018), and cave microclimate and dripwater chemistry monitoring (Baker et al., 2014; Treble et al., 2015; Duan et al., 2016), however, allow for statistically robust time series comparisons and can substantially improve our ability to disentangle climatic influences from site-specific processes across disparate climate zones (Fohlmeister et al., 2017).

Depending on the specific site, some proxies may be easier to interpret than others. As such, carbon isotope sometimes need to be pre-constrained through the help of other proxies, e.g. $\delta^{18}O$, to determine dominant processes (Fohlmeister et al., 2017). However, speleothem oxygen isotopes can carry a less straightforward signal than carbon isotopes where overlapping processes in specific regions complicate the $\delta^{18}O$ interpretation (Scholz et al., 2012; Ridley et al., 2015), especially during large climate changes such as the deglaciation (Genty et al., 2006). Studies considering both isotopes profited from the two proxies' mutual information on fractionation processes and were able to disentangle the encoded climatic signal, e.g. between speleothem $\delta^{18}O$ for temperature and speleothem $\delta^{13}C$ for vegetation changes (Fohlmeister et al., 2017; Baker et al., 2017; Novello et al., 2019, 2021; Voarintsoa et al., 2017).

The climatic interpretation of isotopes in speleothem records, as well as in other paleoclimate archives, are not always straightforward and provide only incomplete information and constraints on the dynamics of the Earth's climate system. Climate models with incorporated SWI are another tool to better understand the climate system, and are particularly powerful when applied in tandem with geochemical proxy records (Comas-Bru et al., 2019; PAGESHydro2k-Consortium, 2017). Incorporating SWI within the Earth's hydrological cycle in atmospheric general circulation models (AGCM), atmosphere-ocean general circulation models (AOGCM), and the most complex Earth system models (ESM), is usually done by adding an additional water cycle to the hydrology of the model under explicit consideration of isotopic fractionation processes through H_2O phase transitions (e.g. Tindall et al., 2009; Yoshimura et al., 2008; Werner et al., 2016; Brady et al., 2019; Lewis and Legrande, 2015). This opens the possibility to study and analyze the complete information of the modelled climate system consistent with model physics in past and present climates. Comparing modelled climate to the archived isotopic signatures provides an 'equal ground' comparison opportunity (for example, Werner, 2010; Sturm et al., 2010; Xi, 2014; PAGESHydro2k-Consortium, 2017).

Extensive multi-model comparisons exist for past, present and future as the Paleoclimate Model Intercomparison Project (PMIP, particularly for Jungclaus et al., 2010; Kageyama et al., 2018) under the overarching Climate Model Intercomparison Project (CMIP, particularly for Taylor et al., 2012; Eyring et al., 2016), to better understand the causes of model spreads in future projections and especially in temperature and precipitation. Simulations of the historical period (1850-2014CE, as in Eyring et al. (2016)), or the last millennium (850-1850CE, as in Eyring et al. (2016)) that will be the focus of this study, as well as idealized experiments under a range of natural and external forcings, are evaluated using different variables. SWI, however, have not been included in the CMIP5/CMIP6 assessments (Taylor et al., 2012; Eyring et al., 2016).

The Stable Water Isotope Intercomparison Group (SWING) formed to bridge this gap of systematic intercomparison between isotope-enabled model simulations and compares them to observations over the historical period, while providing a large dataset to the scientific community (Risi et al., 2012). The historical period is, however, too short to analyze and compare multi-decadal to centennial isotopic variability. To evaluate paleoclimate model simulations whilst investigating changes in climate, the combination of SWI from proxy records and model simulations is essential to improve our understanding of climate change and its variability (Phipps et al., 2013).

The Speleothem Isotope Synthesis and Analyses (SISAL) working group has collected a large number of speleothem records globally and compiled the database SISALv2 (Atsawawaranunt et al., 2018; Comas-Bru et al., 2019, 2020b). It has been employed for model-data comparisons of the Last Glacial Maximum, the Mid-Holocene, the last millennium, and the historical period using different models (iCESM: Midhun et al. (2021), iHadCM3: Bühler et al. (2021), ECHAM5-wiso: Comas-Bru et al. (2019); Parker et al. (2021) and GISS-E1-R: Parker et al. (2021)). Previous model-data comparisons supports the use of the database to evaluate modelled $\delta^{18}O$ across different time periods (Comas-Bru et al., 2019), although speleothems exhibit a lower $\delta^{18}O$ variability than simulated $\delta^{18}O$ on interannual to decadal timescales globally (Bühler et al., 2020). However, a benchmarking study on model performance in simulating $\delta^{18}O$ and its variability, including multi-model comparison or model-data comparison with SISALv2 ,has not yet been performed.

Variability in models can either result from internal interactions and processes within the model, or from changes in external radiative forcings (e.g. GHG, volcanoes, and solar irradiance as in Fig. 1). Variability in the speleothem isotopic signal are also be a consequence of climate-related variability in oxygen isotopes as reflected in climate modes (e.g. El-Niño Southern Oscillation (Sun et al., 2018; Midhun et al., 2021), the North Atlantic Oscillation (Scholz et al., 2012) or the Indian summer monsoon (Fleitmann et al., 2007; Neff et al., 2001)) or changes in radiative forcing. Variations in $\delta^{18}O$ and $\delta^{13}C$ are routinely attributed to changes in solar radiation as a consequence of its influence on climate modes of variability, temperature or precipitation (Warken et al., 2021; Lone et al., 2014; Cosford et al., 2008; Neff et al., 2001). While modelled variability commonly underestimates measured variability in paleoclimate archives with increasing discrepancies on longer timescales (Laepple and Huybers, 2014a), cave-internal variability in speleothems may also overlay the archived signal. Especially on

subdecadal to decadal timescales, lag time between the surface rainfall and the cave drip water, as well as the usually slow response of the cave micro-climate to the surface climate, dampens the signal.

Here we will present a multi-model comparison of five isotope-enabled last millennium simulations: ECHAM5/MPI-OM (Sjolte et al., 2018), GISS ModelE2-R (Lewis and Legrande, 2015; Colose et al., 2016a, b), the isotope-enabled version of the Community Earth System Model (Stevenson et al., 2019; Brady et al., 2019), the isotope-enabled version 3 of the Hadley Model (Bühler et al., 2021), and the stable water isotope-incorporated Scripps Experimental Climate Prediction Center's Global Spectral Model (Yoshimura et al., 2008), with climate characteristics and forcings as depicted in Fig. 1 and listed in Tab. 1. This multi-model comparison complements previous work (Jungclaus et al., 2017; Midhun and Ramesh, 2016; Conroy et al., 2013), through its focus on how different models represent SWI and their variability on different timescales over the entire last millennium. We aim to identify common model biases (Kageyama et al., 2018) globally and in different regions, as well as distinguish specific climate drivers for modelled isotope variability on decadal and longer timescales. This allows, for the first time, for the joint intercomparison of SWI variability in climate models and proxy archives in a time period dominated by natural forcing.

The last millennium is a suitable time period for model-data comparisons, as it provides an opportunity to study variability on decadal and longer timescales and to decipher internal from externally forced variability (Kageyama et al., 2018). Boundary conditions such as orbital forcing, sea level, and ice sheets are close to present-day, and external variability is mostly driven by variations in volcanic eruptions (Schurer et al., 2014; Neukom et al., 2019; Legrande and Anchukaitis, 2015). It is a key-paleoclimate period for the CMIP5 and CMIP6 experiments (Taylor et al., 2012; Eyring et al., 2016) and speleothem records are abundant in this period (Bühler et al., 2021).

With this study, we aim to contribute to the understanding of both model and data: a) How do different simulations model oxygen isotopes in the hydrological cycle and how do they compare to archived speleothem data? b) What processes influence speleothem isotope composition and what effects of variability can be captured and later analyzed? We first compare their similarities and differences in the isotopic signatures of precipitation globally (Sect. 4.1) as well as particularly at the cave site locations of a large number of high-resolution speleothems from the SISALv2 database (Comas-Bru et al., 2020b). Through spatial testing of climate variables, we analyze the relationship between the measured stable isotopes of oxygen and carbon and different modelled climate variables (Sect. 4.2). These relationships will help to determine spatial biases between the models and drivers for modelled and recorded isotopes. Temporal coherence between models and data give insight into internal and externally driven climate variability on different timescales. In a second step, we thus investigate if models can reproduce variability as measured in speleothems on annual to centennial timescales (Sect. 4.3). Finally, we test the timescales of externally forced events, e.g. volcanic eruptions or variations in the solar irradiance, that speleothems archives are able to resolve (Sect. 4.4).

2 Data

In this study, we collected and standardized the output from five different isotope-enabled climate model simulations over the last millennium, as well as oxygen and carbon isotopes in speleothems from the SISALv2 database.

2.1 Isotope-enabled general circulation models

A major advantage given by modelling SWI is its ability to both temporally and spatially resolve the variability of isotopes in precipitation by adding $H_2^{18}O$ and HDO to the part which already simulates and traces the most abundant stable water isotope, $H_2^{16}O$. Simulated $\delta^{18}O$ will further be denoted as $\delta^{18}O_{sim}$. In the atmospheric advection scheme of the model, which is generally a part of the model's dynamical core, all three water isotopologues behave identically. In case of a phase transition (such as melting, condensing, evaporating, and freezing), additional fractionation effects are applied to the

two less abundant water isotopologues. These phase changes typically occur in evaporation from land and ocean surfaces, condensation during formation of clouds, rain, snow, and re-evaporation of precipitation below cloud (for example, Werner, 2010; Sturm et al., 2010).

5 The models used in this study range from AGCMs forced with sea surface temperatures and sea-ice distribution to atmosphere-ocean general circulation models (AOGCMs). Their basic characteristics and boundary conditions are listed in Tab. 1. They are both used individually in the analysis, as well as by the ensemble mean of all models. Fig. 1 shows the climate as represented by the different models and external forcings used in the simulations. Since SWING2, there has not been a consistent protocol for simulations with isotope-enabled models. Hence, the simulations used in this study largely follow the PMIP version 3 last millennium experiment protocol (Schmidt et al., 2011, 2012) with its proposed climate forcing 10 reconstructions, with some variations in vegetation and orography. Of the external forcings used, differences in the volcanic forcing may have the largest influence on differences between the simulations (Colose et al., 2016a; Schmidt et al., 2011), as different responses on larger eruptions may have a long term impact. Large eruptions can cause local anomalies to the mean state of $\delta^{18}O$ of up to ± 1.5‰ (Colose et al., 2016a), hinting at the magnitude of change that can be caused by different forcings. Volcanic eruptions are among the most prominent drivers of natural climate variability during the last millenium 15 (Jungclaus et al., 2017). Compared to volcanic forcing, the choice in solar or orbital forcing has a smaller effect over time in the last millennium. Although the simulations do use forcings based on different reconstructions, which then act on various timescales, differences in response may not only arise from forcings but also from their implementation in the models (Jungclaus et al., 2017).

2.1.1 ECHAM5/MPI-OM

20 We use the isotope-enabled version of the fully coupled GCM ECHAM5/MPI-OM (hereafter, ECHAM5-wiso) (Werner et al., 2016; Jungclaus et al., 2006). The model consists of the atmospheric model ECHAM5 (Roeckner et al., 2003) and the ocean model MPI-OM with an embedded sea-ice model (Marsland et al., 2002). The millennium-long simulation by Sjolte et al. (2018) covers the period 800-2000 CE, and uses a similar setup as the E1 COSMOS ensemble by Jungclaus et al. (2010), but with a different solar forcing based on the solar modulation record inferred from combined neutron monitor and 25 tree-ring ^{14}C data (Muscheler et al., 2016).

Isotope diagnostics have been implemented for the atmosphere, ocean, and land surface component of the model and are computed throughout the entire water cycle in the ECHAM5 (Werner et al., 2016) and MPI-OM (Werner et al., 2016) models. The land surface model assumes no fractionation in most of the physical processes (Haese et al., 2013). Water tracers are fully mixed and advected in the ocean model, and the SWIs total mass is conserved (Werner et al., 2016).

30 ECHAM5-wiso has been used extensively within the paleoclimate field, as well as for present time (for example, Werner et al., 2016; Langebroek et al., 2011; Goursaud et al., 2018). The fully coupled GCM version of the model ECHAM5/MPI-OM has good agreement with both present-day isotope observations from the GNIP database, as well as with ice core and speleothem proxies during mid-Holocene (Comas-Bru et al., 2019), Last Glacial Maximum (Werner et al., 2016; Comas-Bru et al., 2019), and for the last interglacial (Parker et al., 2021). Both in the GCM and with the atmospheric component 35 (ECHAM5-wiso), a warm bias in the model is found over high-latitudinal regions, especially over Greenland and Antarctica (Werner et al., 2011, 2016). This has been attributed to the coarse spatial resolution in the atmospheric component of the model (Werner et al., 2016) resulting in an underestimation of isotope depletion in these regions. The last millennium simulation has not been evaluated globally, but climate reconstructions and variability of SWI have been compared in the North Atlantic region, where the amplitude of the variability was underestimated in the model compared to ice cores (Sjolte 40 et al., 2018). Previous studies also stress the isotopic response to volcanic eruptions and phases of NAO (Guðlaugsdóttir et al., 2018, 2019).
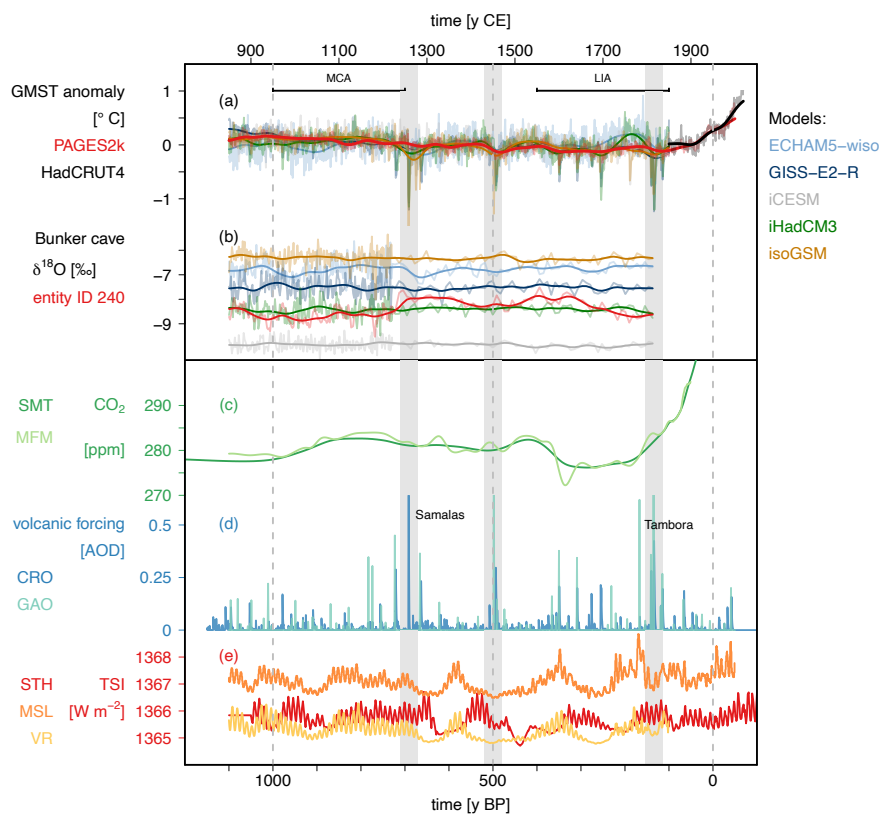
Figure 1. Climate as represented by the different models (ECHAM5-wiso (light blue), GISS-E2-R (dark blue), iCESM (grey), iHadCM3 (green) and isoGSM (orange)) and external forcings over the last millennium: a) Global mean surface temperature anomaly as represented by the models (in model colors) relative to the period of the last millennium (850-1850CE), as well as the reconstructed temperature anomaly (PAGES2k, red, PAGES2k-Consortium, 2019), and observed temperatures (HadCRUT4, black, Morice et al., 2012)). b) Isotopic composition of precipitation in the different models (in model colors) at the cave site location of Bunker cave (Germany) including the $\delta^{18}O_{speleo}$ of entity ID 240 (red), all at the temporal resolution of entity ID 240 (Comas-Bru et al., 2020b; Fohlmeister et al., 2012). For both temperature and $\delta^{18}O$, we show the annual and down-sampled values in lighter colors in the background. Bold colors show the values with a 100 yr Gaussian kernel bandpass (Rehfeld and Kurths, 2014). c) Atmospheric CO_2 concentration (SMT: Schmidt et al. (2012), MFM: MacFarling Meure et al. (2006)). d) Volcanic forcing in units of aerosol optical depth (AOD) (CRO: Crowley et al. (2008); Crowley and Unterman (2013), GAO: Gao et al. (2008)), where the AOD for the Gao et al. (2008) reconstruction was estimated by dividing the sulfate loading by 150 Tg (following Atwood et al., 2016). e) Total solar irradiance (TSI) (STH: Steinhilber et al. (2009), MSL: Muscheler et al. (2016), VR: Vieira, L. E. A. et al. (2011)). The grey bars mark particular periods of high volcanic forcing.

Table 1. Basic characterization of the last millennium simulation.

	ECHAM5/MPI-OM	GISS ModelE2-R	iCESM1	iHadCM3	isoGSM
Reference	Sjolte et al. (2018); Werner et al. (2016)	Lewis and Legrande (2015); Colose et al. (2016a, b)	Brady et al. (2019); Stevenson et al. (2019)	Bühler et al. (2021); Tindall et al. (2009)	Yoshimura et al. (2008)
Years	800-2005 CE	850-1979 CE	850–2005 CE	850-1850 CE	851-2000 CE
Atmospheric model resolution	$3.75° \times 3.75°$ with 19 vertical levels	$2.5° \times 2°$ with 40 vertical levels	$2.5° \times 1.875°$ with 30 vertical levels	$3.75° \times 2.5°$ with 19 vertical levels	$1.875° \times 1.875°$ with 28 vertical levels
Orography	fixed to 1950 CE	ETOPO1 (NOAA National Geophysical Data Center, 2009; Amante and Eakins, 2009) fixed to 1950 CE	GTOPO30 (Gesch et al., 1999) fixed to 1950 CE	fixed to 1950 CE	ETOPO5 (National Geophysical Data Center, 1993) fixed to 1950 CE
Orbital Parameter	Variation Seculaires des Orbites, Planetaires (VSOP) analytical solution by Bretagnon and Francou (1988)	Berger and Loutre (1991)	Berger (1978)	fixed to 1950 CE	a millennium trend is considered
GHG	CO_2, CH_4, NO_2: MacFarling Meure et al. (2006), Historical, anthropogenic: Marland et al. (2003), Ozone: Climatology of Paul et al. (1998)	Transient from 850 CE (Schmidt et al., 2011)	well-mixed greenhouse gases (CO_2, CH_4, NO_2) from high-resolution Antarctic ice cores (Schmidt et al., 2011)	well-mixed CO_2, CH_4, NO_2 and other trace gases (Schurer et al., 2014; Schmidt et al., 2012)	well-mixed greenhouse gases (CO_2, CH_4, NO_2) from high-resolution Antarctic ice cores (Schmidt et al., 2012)
Land cover	Pongratz et al. (2008) with vegetation from Jungclaus et al. (2010)	Pongratz et al. (2008)	Pongratz et al. (2008), starting 1500 CE: Hurtt et al. (2011)	dynamic vegetation TRIFFID (Cox, 2001)	Pongratz et al. (2008), starting 1500 CE: Hurtt et al. (2011)
Volcanic forcing	Crowley et al. (2008)	Crowley et al. (2008)	Gao et al. (2008)	Crowley and Unterman (2013)	Gao et al. (2008)
Total Solar Irradiance	Muscheler et al. (2016, 2007)	Steinhilber et al. (2009), starting 1850 CE: Wang et al. (2005)	Vieira, L. E. A. et al. (2011) with 11-year cycle added similar to Schmidt et al. (2011)	Steinhilber et al. (2009); Wang et al. (2005); Schurer et al. (2014)	Vieira, L. E. A. et al. (2011), starting 1834 CE: Lean (2009), with 11-year cycle added from Schmidt et al. (2012)

2.1.2 GISS ModelE2-R

The isotope-enabled AOGCM GISS ModelE2-R (hereafter, GISS-E2-R) (Schmidt et al., 2006, 2014) is used with the same physics as in the CMIP5 experiments (Miller et al., 2014; Schmidt et al., 2014). Water tracers and isotopes are incorporated into the atmosphere, land surface, ocean, and sea-ice components of the model (Schmidt et al., 2005). Several experiments

5 have been set up for the last millennium with GISS-E2-R, due to uncertainties in past forcings and their effects, with different combinations of solar, volcanic, and land-use/vegetation forcings but all with the same greenhouse gas and orbital change (Colose et al., 2016a, b; Lewis and Legrande, 2015).

GISS-E2-R has been shown to simulate modern observations of SWI well, except over Antarctica, in terms of changes in convection, clouds, and isotope kinetics (Schmidt et al., 2005). For the last millennium, GISS-E2-R has also explored the

10 isotopic responses to volcanic eruptions in South America (Colose et al., 2016a), volcanic forcing in relation to the position of the intertropical convergence zone (Colose et al., 2016b), and to ENSO (Lewis and Legrande, 2015). The model has been

shown to have a warm sea surface temperature bias and issues in sea ice concentration around Antarctica, related to the transport of the Antarctic Circumpolar Current. In the tropics, a warm bias is also found over land, together with cooler northern midlatitudes (Schmidt et al., 2014).

2.1.3 iCESM1

5 We use the last millennium run of the isotope-enabled AOGCM iCESM1 version 1.2 model (hereafter, iCESM) (Hurrell et al., 2013; Brady et al., 2019; Midhun et al., 2021), a fully-forced simulation out of an eight-member ensemble of different external forcings. As the model is open-source and publicly available, it is widely used in the scientific community, and simulations for past (Zhu et al., 2017; Zhang et al., 2012) and present climate exist (Otto-Bliesner et al., 2016).

The model consists of the isotope-enabled Community Atmosphere Model version 5.3 (iCAM5.3, isotope-enabled version
10 based on Neale et al., 2010), a Land Model CLM4 (Oleson et al., 2010), a sea-ice model, and an ocean component that is based on the isotope-enabled POP2 (Zhang et al., 2017). Isotopes in the water cycle are represented as a new parallel hydrological cycle in all hydrological components in the atmosphere, ocean, land, and sea ice in the form of numerical water tracers and can be tracked in space and time.

The isotope-enabled version captures general global isotopic signatures well over ocean areas but shows small discrep-
15 ancies across the land surface (Brady et al., 2019). This effect has been explained by the model showing a slight negative isotopic bias due to overestimated modelled convection in mid-latitude oceans. Consequently, the transport of SWI-mass poleward and landward has been deemed insufficient (Nusbaumer et al., 2017). Footprints associated with major climatic modes such as ENSO and PDO are found to be well represented also in isotopic signatures (Midhun et al., 2021).

2.1.4 iHadCM3

20 We use the last millennium run from the fully coupled isotope-enabled AOGCM iHadCM3 (Bühler et al., 2021). iHadCM3 has been widely used to simulate present (Dalaiden et al., 2020) and future climate (Sime et al., 2008; Tindall et al., 2009; IPCC, 2013), as well as for past climates (Tindall et al., 2010; Sime et al., 2013; Holloway et al., 2018). The model consists of several components: the atmosphere model HadAM3 (Pope et al., 2000), the ocean model HadOM3 (Gordon et al., 2000), a sea ice model (as described in Valdes et al., 2017) and a dynamic land surface and vegetation model (Cox, 2001).

25 For the isotope-enabled version, SWI were added as two separate water species in the atmospheric model, and as tracers in the ocean model. Fixed isotope fractions are added to a fixed volume gridbox of the ocean and experience changes due to evaporation, precipitation, and runoff through a virtual flux of SWI, altering the $\delta^{18}O_{sim}$ ratio in the top level of the ocean accordingly (Tindall et al., 2009).

Compared to instrumental observations, the model represents sea surface temperature, ice sheet, and ocean heat content
30 well (Gordon et al., 2000). The freshwater hydrological cycle in the model shows only a slight overestimation in the local evaporation (Pardaens et al., 2003). The model simulates the major isotopic fractionation effects defined by Dansgaard (1964) (e.g. the latitude effect, the amount effect, and the continental effect) appropriately compared to GNIP data (Zhang et al., 2012). Additionally, a broad agreement in isotopic output with GNIP data in the general spatial distribution can be observed (Tindall et al., 2009).

2.1.5 isoGSM

35 IsoGSM is the isotope-enabled version of the AGCM Scripps Experimental Climate Prediction Center's (ECPC) Global Spectral Model (hereafter, isoGSM) (Yoshimura et al., 2008). The model is based on the previous medium-range forecast model used at NCEP, making it well documented in its performance as an operational weather forecast model (Kanamitsu et al., 2002; Caplan et al., 1997).

The IsoGSM is a stand-alone atmospheric model. Here, it has been forced with sea surface temperatures and sea-ice distributions from the CCSM4 last millennium simulation (Landrum et al., 2013). Land surface processes are modelled through the NOAH model, but isotopic fractionation is not considered in these processes (Yoshimura et al., 2008).

isoGSM has shown to represent isotope and precipitation observations globally using a spectral nudging technique captured by the NCEP/DOE Reanalysis dataset (Yoshimura et al., 2008). Its last millennium simulation has not been evaluated in previous studies, but isoGSM captures large-scale isotope and climate patterns in present times (Risi et al., 2012). The model has shown to also reproduce observed isotopic and precipitation variability well over the regions of Indian Summer Monsoon (Berkelhammer et al., 2012a), western North America (Berkelhammer et al., 2012b), and NW Scotland (Baker et al., 2012). Recently, IsoGSM showed good consistency with speleothem oxygen isotopes from East Asia (Chiang et al., 2020) and from South Asia (Kathayat et al., 2021). isoGSM tends to underestimate the depletion of $\delta^{18}O_{sim}$ in dry regions such as Antarctica (Yoshimura et al., 2008). A decreasing summer temperature increases the precipitation $\delta^{18}O_{sim}$, and is caused by the moisture transport scheme of the model associated with areas of extremely dry conditions (Yoshimura et al., 2008; Risi et al., 2012).

2.2 SISALv2 database
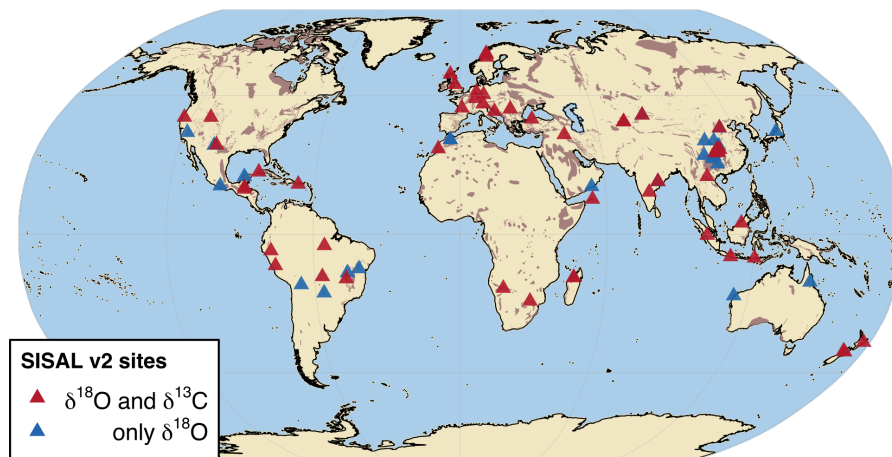
Figure 2. Site locations of the SISALv2 database on a global karst map (brown shading by Williams and Ford (2006). We only consider entities that cover a minimum of 600 year period within the last millennium and that include at least 2 dates and 36 isotopic measurements in this period. Shown are all sites within the last millennium meeting these selection criteria that have both oxygen and carbon isotope measurements (red), and only oxygen isotopes measurements (blue).

In this study, we use speleothem data from the Speleothem Isotope Synthesis and Analysis version 2 (SISALv2) database (Atsawawaranunt et al., 2018; Comas-Bru et al., 2019, 2020a, b). The database includes 691 speleothem records from 294 caves across the globe, from all continents except Antarctica. The last millennium has abundant records globally with sufficient resolution and reasonable dating uncertainties (Bühler et al., 2021). We filtered the database for records that cover at least a 600 yr period within the last millennium (850-1850CE), exhibit at least two dates and 36 stable isotope measurements within the time period, to guarantee a minimum resolution of 30 yr. We obtain 89 records from 75 different sites for $\delta^{18}O_{speleo}$ of which 58 records (65 %) from 50 sites also have $\delta^{13}C_{speleo}$ measurements (Fig. 2).

3 Methods

To compare climate simulation outputs and speleothem data, both need some preparation. Modelled output comes in regular monthly resolution, while time series of speleothem proxies are irregularly sampled. Different speleothem mineralogies, as well as different isotopic standards between modelled and recorded data, need to be accounted for before statistical similarity measures are applied.

3.1 Speleothem drip water conversion

The database includes calcite, aragonite, and mixed mineralogy speleothem records. Following Comas-Bru et al. (2020b), we only use pure calcite or aragonite speleothems in our analysis. Stable isotope ratios are usually given in δ-notation, with stable oxygen isotopes as $\delta^{18}\mathrm{O} = \left(\frac{\frac{^{18}\mathrm{O}}{^{16}\mathrm{O}}\text{ sample}}{\frac{^{18}\mathrm{O}}{^{16}\mathrm{O}}\text{ standard}} - 1 \right) \cdot 1000\ \text{‰}$, with the standard denoting either the Vienna Standard Mean Ocean Water (V-SMOW, Dansgaard, 1964; Kendall and Caldwell, 1998) for water in its liquid and gaseous phases, or Vienna Pee Dee Belemnite (V-PDB, Coplen et al., 1983) for $\mathrm{CaCO_3}$. The stable carbon isotope ratio is denoted as $\delta^{13}\mathrm{C} = \left(\frac{\frac{^{13}\mathrm{C}}{^{12}\mathrm{C}}\text{ sample}}{\frac{^{13}\mathrm{C}}{^{12}\mathrm{C}}\text{ standard}} - 1 \right) \cdot 1000\ \text{‰}$, against the V-PDB (Coplen, 1995).

To be able to compare precipitation $\delta^{18}\mathrm{O}_{sim}$ values to those measured in calcite or aragonite, the $\delta^{18}\mathrm{O}_{speleo}$ is converted to its *drip water equivalent* ($\delta^{18}\mathrm{O}_{dweq}$) relative to the V-SMOW standard as in Comas-Bru et al. (2019). This conversion is temperature dependent but to different extents for both minerals. Tremaine et al. (2011) provide an empirically based fractionation formula for speleothems of calcite mineralogy:

$$\delta^{18}\mathrm{O}_{\mathrm{dweq}} = \delta^{18}\mathrm{O}_{\mathrm{calcite}} - \left(\left(\frac{16.1 \cdot 1000}{T} \right) - 24.6 \right), \tag{1}$$

where T is the temperature in K and $\delta^{18}\mathrm{O}$ are given in units of ‰.

Aragonite speleothems form under different conditions, e.g. higher Mg content of the dripping solution or slow drip-rate (Fairchild and Baker, 2012), resulting in a different fractionation factor compared to calcite as described by Grossman and Ku (1986):

$$\delta^{18}\mathrm{O}_{\mathrm{dweq}} = \delta^{18}\mathrm{O}_{\mathrm{aragonite}} - \left(\left(\frac{18.34 \cdot 1000}{T} \right) - 31.954 \right). \tag{2}$$

For both conversions, the cave temperature at the time of the fractionation is needed. As these are often not available, especially in a palaeoclimate setting, we use annual mean modelled surface temperatures as a surrogate for cave temperatures (Fairchild and Baker, 2012). For caves in very cold conditions, the annual mean surface temperature may underestimate the mean cave temperature by some degrees due to long-lasting snow-packs. This underestimation, however, only corresponds to an overestimation of 1 ‰ in $\delta^{18}\mathrm{O}_{dweq}$ and is within the range of the simulation ensemble. Additionally, cave-dependent time lags between the surface and the cave temperature are not accounted for, as they have a negligible effect on the time-averaged mean isotopic value. The conversion to drip water equivalent is done for each entity and each simulation individually, where we use the simulated annual mean surface temperature, down-sampled to the record's resolution.

In a last step, the V-PDB values are converted to V-SMOW for direct comparison to the modelled SWI, using the conversion from Coplen et al. (1983):

$$\delta^{18}\mathrm{O}_{\mathrm{SMOW}} = 1.03092 \cdot \delta^{18}\mathrm{O}_{\mathrm{PDB}} + 30.92. \tag{3}$$

For carbon isotopes, different fractionation paths exist depending on mineralogy. Following Fohlmeister et al. (2020), we convert the aragonite $\delta^{13}\mathrm{C}$ values to corresponding calcite values using a fractionation offset of 1.9 ± 0.3 ‰ ($\delta^{13}\mathrm{C}_c = \delta^{13}\mathrm{C}_{calcite} = \delta^{13}\mathrm{C}_{arag} - 1.9 \pm 0.3$ ‰). This offset accounts for the different enrichment-factors of the two polymorphs as established in laboratory studies (Romanek et al., 1992) and confirmed in a speleothem study (Fohlmeister et al., 2018).

From the drip water conversion, we obtain a matrix for each of the isotopes with one row per measurement and six columns, where one represents the observations and the other five the modelled estimates.

3.2 Data processing

The simulation output from the five different climate models is available at monthly resolution but with differing time coverage. All simulation runs are cut to cover the time period from 850 to 1850 CE, an interval that is similar to PMIP's interval in the last millennium experiment. We focus on surface temperature, precipitation, precipitation-$\delta^{18}O_{sim}$, and evaporation. For the simulations lacking evaporation as a diagnostic (iCESM, isoGSM, and iHadCM3), we convert latent heat to potential evaporation and use these variables within the simulations. Outliers in the simulation are removed by comparing each modelled value in the 3D-output data matrix with its eight neighbors in time and space. If the value deviates from the mean of these eight values by more than five standard deviations, the value is set to NA. On average 0.001% of values are set to NA through this method.

$\delta^{18}O_{speleo}$ forms from drip water that reaches the cave, which can be approximated by calculating the difference between precipitation amount and evaporation. When comparing modelled to speleothem isotopes it is, therefore, more realistic to weight the modelled $\delta^{18}O_{sim}$ by precipitation minus evaporation amount (infiltration adjusted precipitation weighting, *iw*) to obtain annual $\delta^{18}O_{sim}$ values. The weighting automatically focuses on the local seasonal composition of SWI in rainfall, and prevents bias towards seasons with minimal infiltration due to high evaporation. Weighted $\delta^{18}O_{sim}$ values are commonly used in speleothem model-data comparison studies (Comas-Bru et al., 2019; Baker et al., 2019). The simulated weighed $\delta^{18}O$ mean is calculated as:

$$\delta^{18}O_{iw} = \frac{\sum_1^n \delta^{18}O_k iw_k}{\sum_1^n iw_k} \tag{4}$$

where $\delta^{18}O_{iw}$ is the monthly weighted annual composition of isotopes, $\delta^{18}O_k$ refers to monthly simulated $\delta^{18}O$ and iw_k is the corresponding monthly amount of *iw*, where $n = 12$. As isotopic fractionation also occurs during evaporation from the soil, models, where $\delta^{18}O_{sim}$ is also available for soil layers, would be more realistic to compare to speleothem data. However, these were only available for a few simulations. Using $\delta^{18}O_{sim}$ of precipitation for the calculation of $\delta^{18}O_{iw}$, therefore, offered a more equal handling of the data while maintaining the large ensemble and enabled a better comparison of results.

Where simulation data are compared on a gridbox-level, we block-average all simulations to the same spatial resolution as that of the ECHAM5-wiso-run, which has the lowest spatial resolution. Data at the speleothem cave sites are extracted via bi-linear interpolation as in Bühler et al. (2021). Here, a gridbox of the size of the simulation's original resolution with the cave's location at its center is resampled from the original gridboxes it overlaps with. We note that this bi-linear interpolation can, however, influence the temporal variability or the values of the response variables (Latombe et al., 2018).

The simulated monthly temperature, precipitation, and evaporation at the speleothem cave locations are averaged to annual mean values. All speleothems in our last millennium subset, however, come as irregularly sampled time series with a median resolution of 5.19 yr per entity (90% CI: 4.13, 6.99). Considering only the speleothems with measurements of both isotopes yields a median resolution of 6.08 yr (4.07, 7.85). To adjust the model and speleothem data, the simulated variables of all models are block-averaged to the irregular temporal resolution of the individual speleothem. We also include speleothems in our analysis where no $\delta^{13}C$ measurements but only $\delta^{18}O$ are available. In direct comparisons between carbon and oxygen isotopes, we only consider those 58 speleothems that provide samples for both isotopes.

The relationship between $\delta^{18}O_{speleo}$ and simulated climate variables is determined following three different latitude bands to guarantee enough data points within each climate zone, the tropics, the subtropics, and the extratropics (Holden, 2012). The tropics are commonly defined as the zone between the Tropic of Cancer and the Tropic of Capricorn (23.44°S to 23.44°N); the subtropical region 23.44 to 35°N/S, and the extratropical region 35 to 90°N/S (with cave sites only extending to 66°N and 42°S).

Spatial testing between speleothem $\delta^{18}O_{dweq}$, $\delta^{13}C_c$, simulated $\delta^{18}O_{sim}$, and meteorological variables is done by linear regression of the simulated millennium mean, down-sampled to the temporal resolution of each record, and entity mean. To account for the spread between simulated variables and calculated $\delta^{18}O_{dweq}$, the linear regression is done via bootstraping ($n = 2000$). Confidence intervals for all entity mean variables are also calculated via bootstrapping with a significance level of $\alpha = 0.1$. p-values are calculated through a fit linear regression model (`fitlm.m` (MATLAB, 2018)) using Pearson's product moment correlation.

Correlation estimates and p-values for regular time series, i.e. the annual resolution output of the simulation, are calculated via the Pearson's product moment correlation (via the function `cor.test` (R Core Team, 2020b)). We use a significance level of $\alpha = 0.1$.

Correlation estimates for irregular time series are calculated via Pearson correlation as adapted by Rehfeld and Kurths (2014) and tested for last millennium speleothem records in Bühler et al. (2021). Here, we also choose a significance level of $\alpha = 0.1$. This level is appropriate for both the regular and irregular time series, considering the number of samples N compared to the strictness and expected level of false positives. Whenever calculating correlation estimates where speleothem data is involved, we use the raw $\delta^{18}O_{speleo}$ or $\delta^{13}C_{speleo}$ instead of the drip-water converted values to decrease any potential biases.

With all simulated variables down-sampled to the irregular resolution of each speleothem record, the use of power spectral analysis of the time series can describe the variation of common signals on a frequency spectrum of all time series (Chatfield, 2003). The *power spectral density* (PSD) of a time series describes the power distribution versus frequency over a finite interval of time (Chatfield, 2003).

To compute spectra of irregularly sampled time series, these are first interpolated to their mean resolution by a double interpolation and filtering process (following Laepple and Huybers, 2014a; Rehfeld et al., 2018; Dolman et al., 2020). This interpolation is performed to reduce high-frequency artifacts. The robustness of this spectral estimation process was recently confirmed by Hébert et al. (2021).

3.3 Synchronous extreme events in speleothem isotopes

An alternative similarity measure to correlation estimates, especially given the irregularity of the available time series, is checking for synchronous extreme events within two time series. After distinguishing extreme events, strength and direction of synchronous extreme events are only based on their relative timing (Rehfeld and Kurths, 2014). In this study, we only focus on the relative timing of the distinguished extreme events to each other.

Within the modelled or measured isotope time series, we distinguish the 5% extreme values as the values above/below the 97.5% / 2.5% quantile of the time series distribution. Two extreme values occurring in a row are treated as two separate extreme events. Extreme values for time series of solar irradiance are determined in the same manner. For the volcanic forcing time series, we distinguish those events above the 95% quantile of the distribution.

Two events are considered synchronous, if they both occur within a time period around the events, limited by a local threshold τ. This local threshold is calculated for each possible pair of extreme events and is chosen as half the minimum time between either extreme event and its preceding or succeeding extreme. For our dataset, the median τ is 4.62 yr (90% CI: 4.37, 5.28), which is of the same order of magnitude as the median resolution of all records with both carbon and oxygen measurements of 6.08 yr, (4.07, 7.85). We set a hard threshold limit of 50 yr, corresponding to the median age uncertainty considering the original chronologies as well as the SISALv2 ensemble chronologies (Comas-Bru et al., 2020b). When

comparing synchronous events between isotopes within one particular speleothem, age-uncertainties are negligible in the comparison as $\delta^{13}C_{speleo}$ and $\delta^{18}O_{speleo}$ values stem from the same measurement of individual sub-samples.

For comparable extreme event signatures between the modelled and measured isotopes to volcanic or solar forcings, each modelled time series is checked for synchronicity against their respective forcing time series. The analysis is repeated for the speleothems for the same number of forcings and averaged.

When looking at the temporal distribution of global synchronous extreme events, they are sorted into bins of 10 yr, which is approximately twice the median local τ. If a pair shows several extreme events within one bin, it is only counted once. We determine significance by randomly permuting one of the time series of a pair and repeating the analysis 2000 times. Within one bin, all counts that are larger than the 95% quantile of this 'mean background noise' can be regarded as significant.

4 Results

4.1 Overview of simulated vs. measured speleothem oxygen isotopes
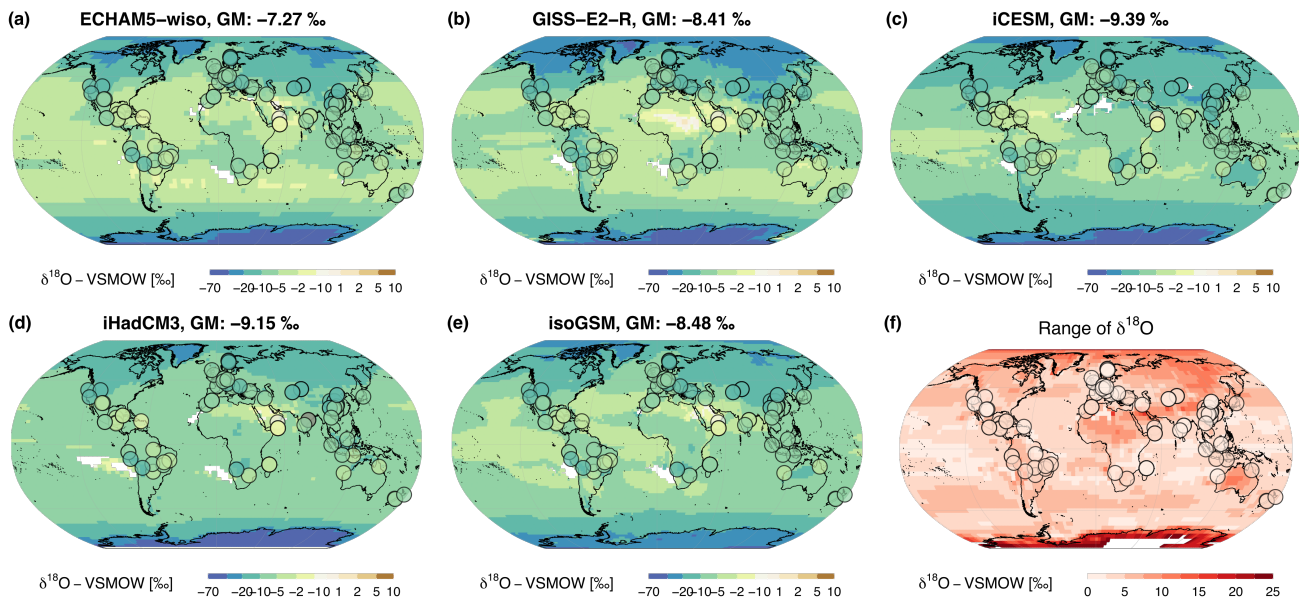
Figure 3. Simulated $\delta^{18}O_{iw}$ climatology (a-e) of the respective simulation: a) ECHAM5-wiso, b) GISS-E2-R, c) iCESM, d) iHadCM3, e) isoGSM) in the background. The time-averages mean $\delta^{18}O_{dweq}$ using the respective simulated temperatures are depicted as circles. Global means (GM) of $\delta^{18}O_{iw}$ are given in the title of each subplot. f) shows the range of $\delta^{18}O_{iw}$ between all simulations for each gridbox, as well as the range for the difference between simulation and record. Light colors indicate large agreement between the simulations, while darker colors mark areas, where the models differ strongly and the spread between the $\delta^{18}O_{iw}$ is larger. Antarctic $\delta^{18}O_{iw}$ ranges are up to 40‰, highlighting the different model performance in this region (white area in f).

We first compare the mean $\delta^{18}O_{iw}$ signal of the five different last millennium simulations, to see potential model biases and large differences between the simulations (Fig. 3 and SFig. 1). The global mean $\delta^{18}O_{iw}$ values are fairly similar in area-weighted global mean of -8.48‰ (90% CI: -8.61, -8.36) and -8.41‰ (-8.62, -8.2) for isoGSM and GISS-E2-R, respectively. The ECHAM5-wiso run is less depleted with a global $\delta^{18}O_{iw}$ mean of -7.27‰ (-7.46, -7.09), and with visibly less depleted mid-latitude oceans than in the other simulations. iCESM and iHadCM3 show a stronger depletion of -9.39‰ (-9.51, -9.28) and -9.15‰ (-9.29, -9.01) respectively, with iCESM showing stronger depletion in the mid-latitudes and iHadCM3 towards the Antarctic compared to the other simulations. Although GISS-E2-R shows strong depletion especially in the arctic region, the less depleted mid-latitudes dominate the global mean (see SFig 1).

This general offset between the global mean $\delta^{18}O_{iw}$ is also visible when comparing the spread of mean values on a gridbox-level (Fig. 3f), where isotopic signatures differ the strongest in the Antarctic. Restricting the view to low- to mid-latitudes, the largest model data differences are found in the Sahara desert, the Arabian peninsula, the Indian peninsula, and Siberia, where low humidity, high precipitation amount or high continentality are the driving local forces of precipitation

5    $\delta^{18}O$. Also shown in Fig. 3f is the spread between the offsets to the respective $\delta^{18}O_{dweq}$ at the cave locations. A close agreement between the models does, however, not necessarily indicate a good model-data match. It only indicates that the difference to the converted speleothem data are similar between the models. Highest agreement of $2.31\%_o$ range is obtained at Tham Duon Mai Cave in Laos (siteID 293 at 20.75°N, 102.65°E , Wang et al., 2019), while strongest disagreement of a range of $8.14\%_o$ between simulations is at Huangye Cave in China (siteID 17 at 33.58°N, 105.11°E, Tan et al., 2011).
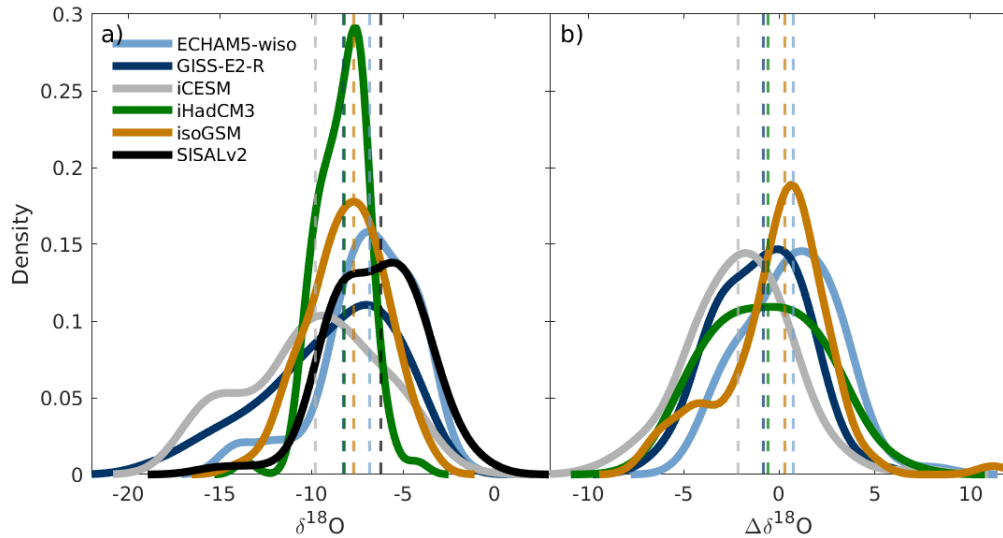
Figure 4. Kernel density estimates of (a) the general distributions in simulated and speleothem $\delta^{18}O$ at cave locations, (b) differences between simulations and speleothems last millennium mean ($\Delta\delta^{18}O= \delta^{18}O_{iw}$ - $\delta^{18}O_{dweq}$). Dashed lines represent the medians.

10   Analyzing the differences between simulations and speleothems can indicate how well the model data matches the proxy signal. Here we investigate the differences in $\delta^{18}O$ between simulated last millennium mean ($\delta^{18}O_{iw}$) and speleothems ($\Delta\delta^{18}O= \delta^{18}O_{iw}$ - $\delta^{18}O_{dweq}$) on a global scale through general distributions, where disagreements between each model and speleothem data are shown as kernel density estimates (Fig. 4). The full datasets are acknowledged through the mean value, whereas the median values exclude skewed distributions and extremes. The speleothem dataset has a median general distri-

15 bution of -6.21‰ globally. Of the simulations, ECHAM5-wiso has the closest distribution median with -6.82‰, followed by isoGSM (-7.72‰), iHadCM3 (-8.20‰), GISS-E2-R (-8.25‰), and iCESM (-9.79‰) (Fig. 4a). The distributions between simulations and speleothem $\delta^{18}O$ (Fig. 4b) are fairly symmetrical but vary between the simulations, with medians of 0.72‰, -0.86‰, -2.01‰, -0.67‰ and 0.28‰, for ECHAM5-wiso, GISS-E2-R, iCESM, iHadCM3 and isoGSM, respectively. While ECHAM5-wiso has the closest median globally, isoGSM has the smallest difference between simulation and speleothem

20    $\delta^{18}O$ at cave locations, with a mean of -0.17‰ (90% CI: $-0.66, 0.33$). GISS-E2-R and iCESM have more negative differences, with a mean of $-1.02\%_o$ $(-1.41, -0.62)$ and $-2.04\%_o$ $(-2.50, -1.60)$, followed by iHadCM3 $-0.68\%_o$ $(-1.18, -0.18)$. ECHAM5-wiso is the only model that has a mean positive difference between simulation and speleothem data, with a mean of $0.63\%_o$ $(0.20, 1.05)$, in line with the less depleted global mean seen in Fig 3.

The largest positive difference (less depleted $\delta^{18}O_{iw}$ than $\delta^{18}O_{dweq}$) is found at Huagapo cave in Peru (siteID 277 at

25 11.27°S, 75.79°W, Kanner et al., 2013) and Minnetonka cave in the USA (siteID 200 at 42.09°N, 111.52°W, Lundeen et al., 2013) for at least four model simulations. Highest negative difference (at least three models agree) are found at Hoq cave on

Socotra Island, Yemen (siteID 253 at 12.59°N, 54.35°E, Van Rampelbergh et al., 2013), Diva cave in Brazil (siteID 38 at 12.38°S, 41.57°W, Novello et al., 2012), and Qunf cave in Oman (siteID 159 at 17.16°N, 54.30°E, Fleitmann et al., 2007).

The general patterns of the isotope climatology are similar between the models (Fig. 3) but can differ at cave locations (SFig. 2). Larger differences in the modelled isotopic signatures appear particularly in regions where modelled temperature spreads widely as well. On average, the differences to the speleothem records (Fig. 4) appear small and are consistent with the general difference to precipitation $\delta^{18}O_{sim}$.
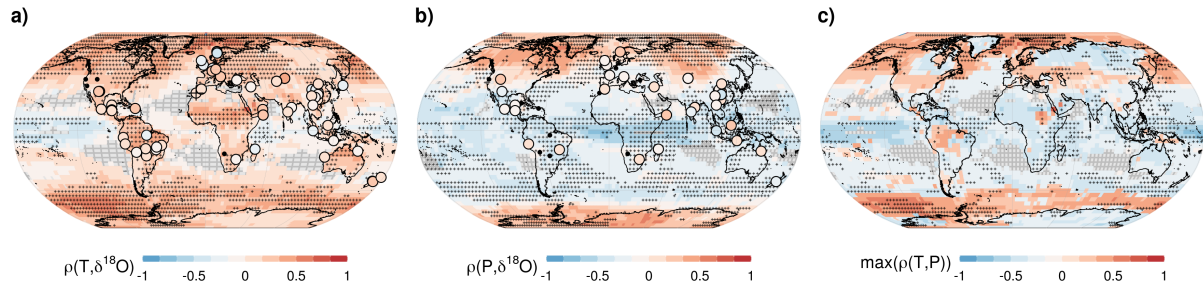
Figure 5. Correlations between SWI and modelled temperature (a) and precipitation (b) time series in each gridbox. The background shows the average over all 5 simulation correlation estimates between annual $\delta^{18}O_{iw}$ and simulated annual temperature per gridbox (a), and for precipitation (b). Crosses indicate gridboxes where correlation estimates for four or more models have the same sign as the averaged estimate over all simulations. Symbols indicate the mean correlation of the simulated temperature (precipitation) of all model simulations to the recorded $\delta^{18}O_{speleo}$ at record resolution. Crossed circles mark sites where more than four models agree in the mean sign of the correlation to $\delta^{18}O_{speleo}$. Black circles indicate the location of those speleothems in the last millennium subset that show no significant correlation to any model. In (c), the map shows positive correlation estimates where $|\rho(\delta^{18}O, T)|$ is larger than $|\rho(\delta^{18}O, P)|$, and vise versa for negative values.

Differences between $\delta^{18}O_{iw}$ signatures between the models may arise from different simulation drivers for the oxygen isotopes, e.g temperature and precipitation, and can hint at different processes that govern the isotopic water cycle at a certain region within the simulations. The mean of the correlation to these main climatic drivers to $\delta^{18}O_{iw}$ shows high agreement between the simulations (Fig. 5, individual correlation fields in SFig. 3). For the correlation to temperature (Fig. 5a), two main domains can be distinguished: there is mainly a positive correlation to temperature in the mid- to high-latitudes and on the continents, and negative correlation in the low-latitude ocean. Large-scale agreement between the simulations is, however, limited to the higher latitudes and the tropical ocean.

Two domains are also apparent in the correlation to precipitation (Fig. 5b), which are even more clearly separated than for temperature. We find areas of negative correlation to $\delta^{18}O_{iw}$ in the low to mid-latitudes and areas of positive correlation only in the high latitudes. The agreement between the simulations, indicated by the crosses, is higher in the low- to mid-latitudes. Combining the information of dominant drivers of $\delta^{18}O_{iw}$ (absolute higher correlation per gridbox in Fig. 5c), we see clear domains of temperature dominance in the Southern Ocean, the higher northern latitudes and some continental regions, while precipitation is more dominant in the lower latitudes, the Antarctic, and Greenland.

The inter-model comparison shows more agreement in the correlation fields to temperature than to precipitation, when focusing only on cave locations: the sign of correlation between $\delta^{18}O_{iw}$ and simulated temperature agree for three and more simulations at 60% of locations, and for four and more simulations at 26% of locations. For precipitation, only 11 % of locations agree in sign for three and more simulations, and only 1.1 % with agreement in four or more simulations. The more uniform temperature response to external forcing may increase the total number of significant correlation estimates and thus also the number of locations that agree in sign.

The model-data comparison shows more significant temporal correlation estimates between simulated temperature to $\delta^{18}O_{speleo}$ and also more sign agreement between these correlation estimates than to simulated precipitation. For precipitation, we find no cave, where more than four models agree in the sign to the mean correlation between modelled and recorded $\delta^{18}O$. For temperature, four speleothems from four different cave sites show a significant correlation of absolute strength 5 $|c| > 0.15$ for at least four simulations.

The data suggests that two main drivers for $\delta^{18}O$ can be distinguished in specific regions - temperature is dominant in the high latitudes, while precipitation appears to be the main driver in the low latitudes. This is what we expected following the principles established by Dansgaard (1964).

4.2 Spatial testing for climatic and environmental effects on speleothem $\delta^{18}O$ and $\delta^{13}C$
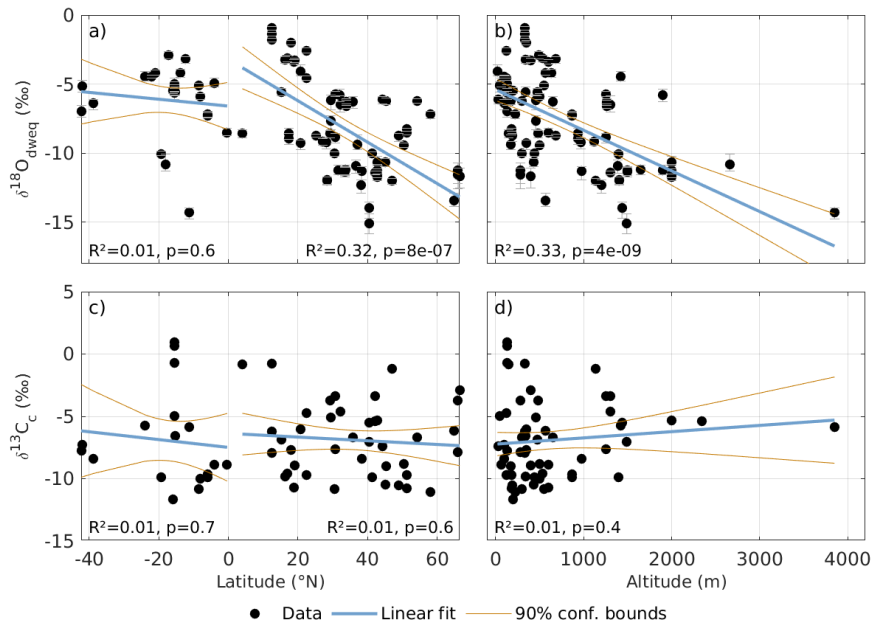
Figure 6. Speleothem $\delta^{18}O_{dweq}$ (first row) and $\delta^{13}C_c$ (second row) against latitude (first column) and altitude (second column) as provided by the SISALv2 database. Linear regression lines are shown separately for northern and southern hemisphere in (a) and (c), while the R^2 and p corresponds to the global linear regressions in (b) and (d). Confidence bounds are 90 %.

10 $\delta^{18}O$ in precipitation shows global signatures depending on latitude or altitude amongst other variables (Dansgaard, 1964). We assess this by looking at the relationships between speleothem $\delta^{18}O_{dweq}$ and $\delta^{13}C_c$ with the site-specific variables of latitude and altitude.

$\delta^{18}O_{dweq}$ decreases as more northern speleothems are considered (hemispherically: Fig. 6a, globally: $R^2 = 0.22$, $p < 0.00$, STab. 1). The large spread in the mid-latitude Northern Hemisphere is mostly due to the high number of speleothem records 15 available in both Europe and China, implying a high longitudinal spread within the database. Fig. 6b) shows a global negative relationship of $\delta^{18}O_{dweq}$ to altitude, even though records get scarcer as the altitude increases. No clear pattern is visible for $\delta^{13}C_c$, and the dataset has a large mean spread (Fig. 6c). A statistically significant relationship between altitude and $\delta^{13}C_c$ cannot be established. However, the spread in $\delta^{13}C_c$ appears to increase with increasing altitude (Fig. 6d), although under decreasing data density.

20 We further explore the simulated meteorological variables and investigate spatial relationships between mean $\delta^{18}O_{speleo}$ and model variable ensemble mean (Fig. 7, STab. 1). We find a significant relationship between $\delta^{18}O_{iw}$ and speleothem $\delta^{18}O_{dweq}$ across all latitude bands (Fig. 7 a-c), with the strongest correlation in the extratropics. Furthermore, we find a
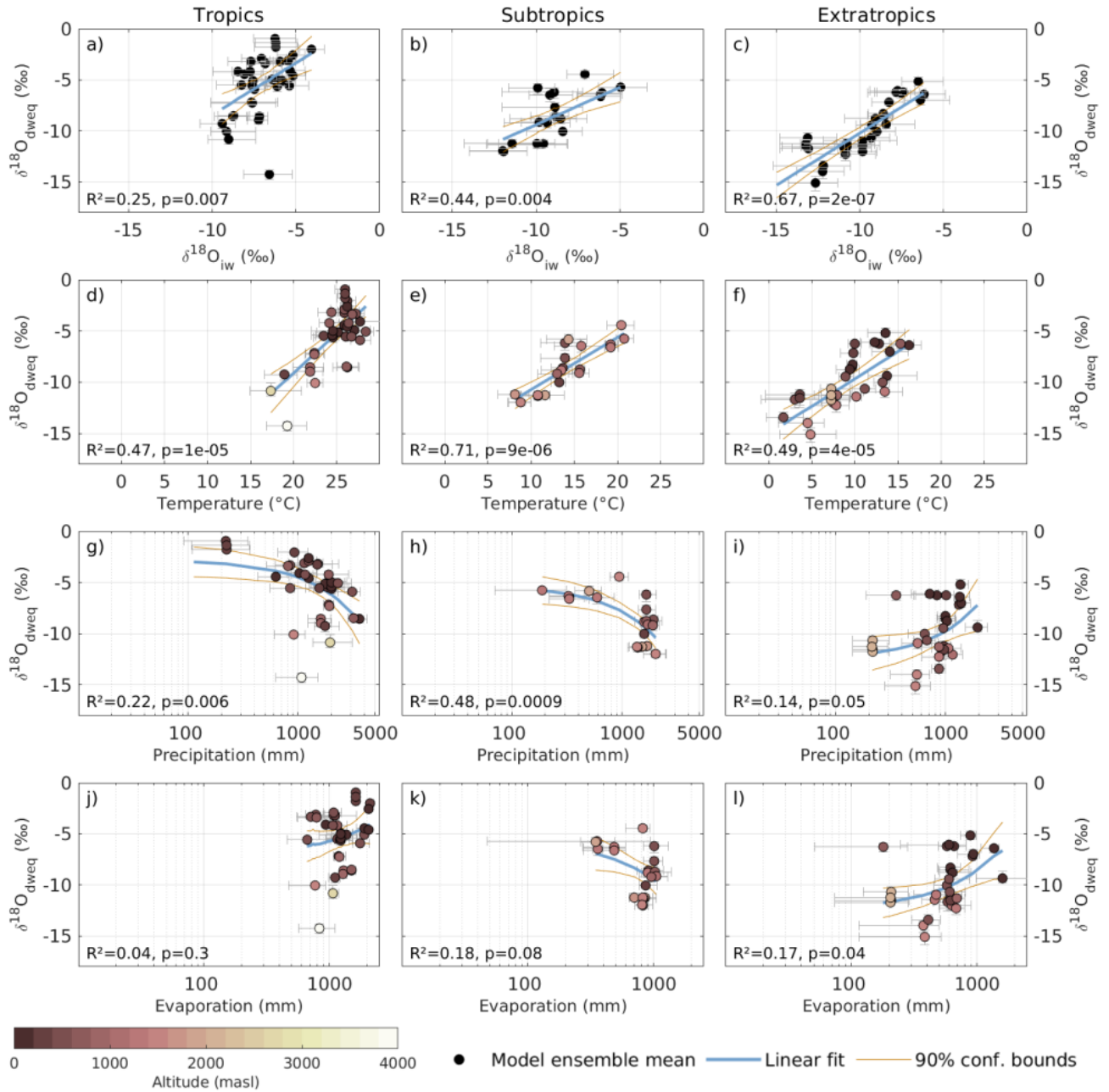
Figure 7. Simulated weighted $\delta^{18}O_{iw}$ (a-c), temperature (d-e), precipitation (g-i) and evaporation (j-l) against speleothem $\delta^{18}O_{dweq}$ for model ensemble mean in the tropics, subtropics and extratropics. The tropical region (23.44°S to 23.44°N) is shown in left panel (a, d, g, j); the subtropical region (23.44–35°N/S) is shown in the middle panel (b, e, h, k); the extratropical region (35–90°N/S) is shown in the right panel (c, f, i, l). Altitude information is applied as shaded colors in d)-l). We use $\delta^{18}O_{iw}$ for all simulations. Note the semi-logarithmic axes for precipitation and evaporation.

global dependency of $\delta^{18}O_{dweq}$ to mean simulated temperature and precipitation at the cave sites. For both temperature and precipitation, we find the strongest relationships to $\delta^{18}O_{dweq}$ in the subtropical regions. In all three regions, the relationship to temperature always exceeds that of precipitation. In Fig. 7 (d-f) cave site altitude information is applied by color codes. This helps in the interpretation of possible overlapping effects of temperature and altitude on $\delta^{18}O$. A significant relationship to annual evaporation can only be distinguished in the extratropical regions (Fig. 7j-l).

We further compare the same meteorological variables to the speleothem $\delta^{13}C_c$ data (Fig. 8, STab. 1). A significant relationship is only found with temperature in the extratropical region (Fig. 8c), with increasing temperatures corresponding
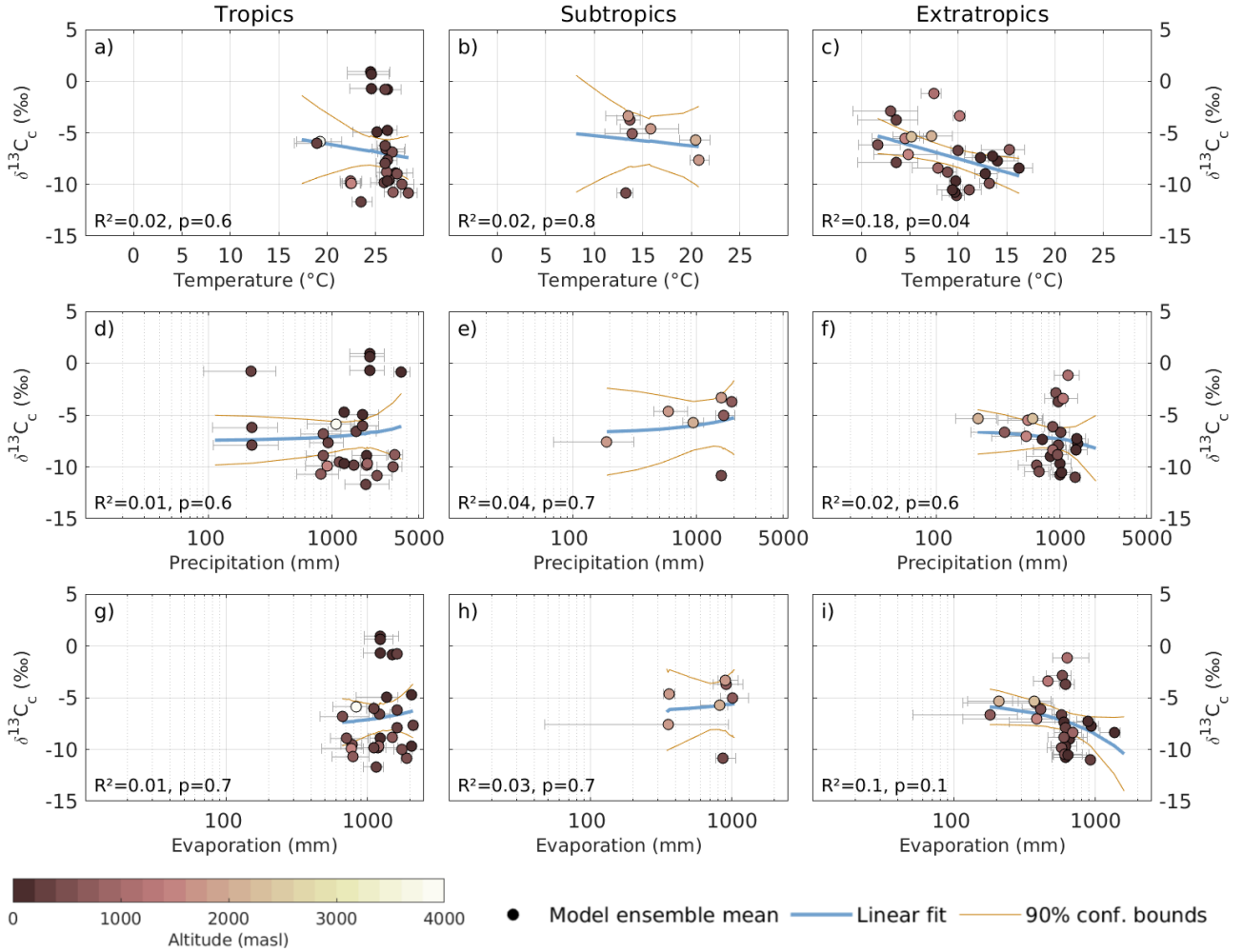
Figure 8. Climate-dependence of carbon isotope variability. Shown are simulated ensemble-mean temperature (a-c), precipitation (d-f) and evaporation (g-i) plotted against speleothem $\delta^{13}C_c$. Altitude information is applied as shaded colors in d)-i). We used linear regressions in all plots, however, these appear curved in a semi-logarithmic plot as used for precipitation and evaporation.

to more depleted $\delta^{13}C_c$. $\delta^{13}C_c$ is also found to be enriched with altitude ($R^2 = 0.23$, p < 0.02, SFig. 4) in the extratropics. This $\delta^{13}C$-altitude relationship is not found in the other latitudinal bands.

The spatial testing shows globally strong relationships between $\delta^{18}O_{dweq}$ to environmental factors, in particular to altitude, temperature, and precipitation, which is in line with previous studies (for example, Comas-Bru et al., 2019; Baker et al., 2019). The spatial relationships between speleothem entity mean $\delta^{13}C_c$ and meteorological variables from model ensemble mean (Fig 8) only show clear relationships in the extratropical region and not on a global scale. This indicates more local influences as discussed by Fohlmeister et al. (2020).

4.3 Variability on different time scales

We compare the variance distribution in oxygen and carbon isotopes over all speleothems. This is a useful measure of how climatic and environmental factors influence the proxies to a different extent. Additionally, different simulations have different representations of variability across different timescales. This behaviour can be explored by calculating power spectral densities (PSD) of the simulated and recorded isotopes averaged globally.

Fig. 9a) provides the spectral ratio of the two isotopes after detrending the irregular time series. A flat spectral ratio of ∼ 1 would indicate same levels of variability for both isotopes on all timescales. The spectral ratio here shows higher variability of
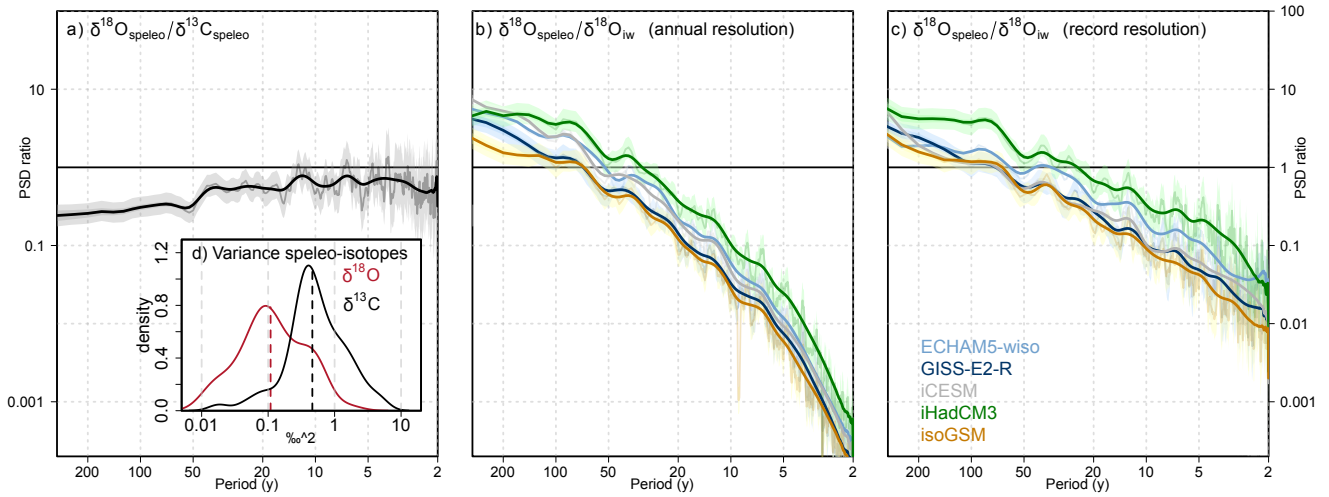
Figure 9. Spectral ratios of isotopes in speleothem and simulation on different timescales as shown by the ratios or mean power spectral densities (PSD): a) spectral ratio between speleothem isotopes (δ^{18}O/δ^{13}C). b-c) spectral ratio over all cave locations for δ^{18}O$_{speleo}$ and δ^{18}O$_{iw}$ per simulation (model-colors). In b) we show the spectral ratios of δ^{18}O$_{speleo}$ to δ^{18}O$_{iw}$ down-sampled to the individual records' resolution and in c) the simulated annually. The full spectra are shown in faded colors and a smoothed spectrum in black or the model colors. d) Variance of detrended δ^{18}O$_{speleo}$ (red) and δ^{13}C$_{speleo}$ (black) as measured in speleothem records. The dashed line indicated the median of the distribution.

δ^{13}C$_{speleo}$ on all timescales, however, for periods smaller than 10 years, the variability of both isotopes is more similar. This is supported by the total variance of the isotopes over the complete period. δ^{13}C$_{speleo}$ shows a much higher total variance with a median of $0.46‰^2$ (0.38, 0.6) compared to δ^{18}O$_{speleo}$ with a median variance of $0.11‰^2$ (0.08, 0.12).

Fig. 9b) shows the measured average PSD of δ^{18}O$_{speleo}$ divided by the simulated average PSD at annual resolution,
5   and Fig. 9c) by the average PSD of δ^{18}O$_{iw}$ at record resolution. A spectral ratio larger than 1 indicates higher variability at the timescale of the recorded δ^{18}O$_{speleo}$, whereas spectral ratios smaller than 1 indicate higher variability of the simulated δ^{18}O$_{sim}$. The spectral ratios between δ^{18}O$_{speleo}$ and simulations at the cave locations at annual resolution show lower variability in δ^{18}O$_{speleo}$ compared to all models on decadal and shorter timescales although to different extents (Fig.9b). When considering the simulations down-sampled to record resolution, the result is similar but there is much lower vari-
10   ability in δ^{18}O$_{speleo}$ at decadal and shorter timescales (Fig.9c). By down-sampling, the simulated spectra lose power on the decadal and shorter timescales, which is then reflected in higher spectral ratios. On decadal to centennial timescales, however, δ^{18}O$_{speleo}$ shows much higher variability than the modelled δ^{18}O$_{sim}$, unaffected by the down-sampling.

Variability of δ^{18}O$_{iw}$ is modelled differently in the simulations, as represented by the different levels of spectral power in the ratios. This difference is supported by the 5 area-weighted global variances of different magnitude, as well as the
15   simulated variance in annual and down-sampled resolution as listed in Tab. 2. Small deviations between calculated variance and variance as area under the PSD can arise from the interpolation before the calculation of the spectra. The general order of isoGSM having the highest and iHadCM3 the lowest power on shorter frequencies remains throughout, as can also be seen in the table with small deviations to the order. The global variance, however, is only partly represented at the cave locations. While isoGSM shows the highest variance globally and at cave locations, iCESM is of medium variance globally but has
20   the smallest variance at cave locations. For unweighted isotopic composition, the order of simulations changes (results not shown).

Table 2. Area weighted mean global $\delta^{18}O_{sim}$-variances as var_{global} with 90% intervals of the distribution are given per simulation. Row two and three give the $\delta^{18}O_{sim}$-variance at the cave locations both in the annual resolution of the simulation, as well as down-sampled to the records resolution.

	ECHAM5-wiso	GISS-E2-R	iCESM	iHadCM3	isoGSM
var_{global}	1.05 (0.15, 2.65)	1.66 (0.19, 10.13)	1.32 (0.07, 4.26)	1.27 (0.13, 5.22)	1.7 (0.16, 4.38)
var_{speleo} (annual)	0.66 (0.22, 2.31)	0.66 (0.17, 3.98)	0.66 (0.07, 3.1)	0.37 (0.16, 1.83)	1.36 (0.21, 9.83)
var_{speleo} (down-sampled)	0.19 (0.03, 1.53)	0.25 (0.02, 1.88)	0.15 (0.01, 2.05)	0.15 (0.02, 1.42)	0.29 (0.03, 8.25)

The analysis suggests that variability in the simulated $\delta^{18}O_{iw}$ is represented differently in the simulations and that the order is not frequency-dependent. The recorded $\delta^{18}O_{speleo}$ shows more variability on centennial and less variability on decadal and smaller frequencies than the simulated, although to a different extent depending on the simulation.

4.4 Analysis of extreme events
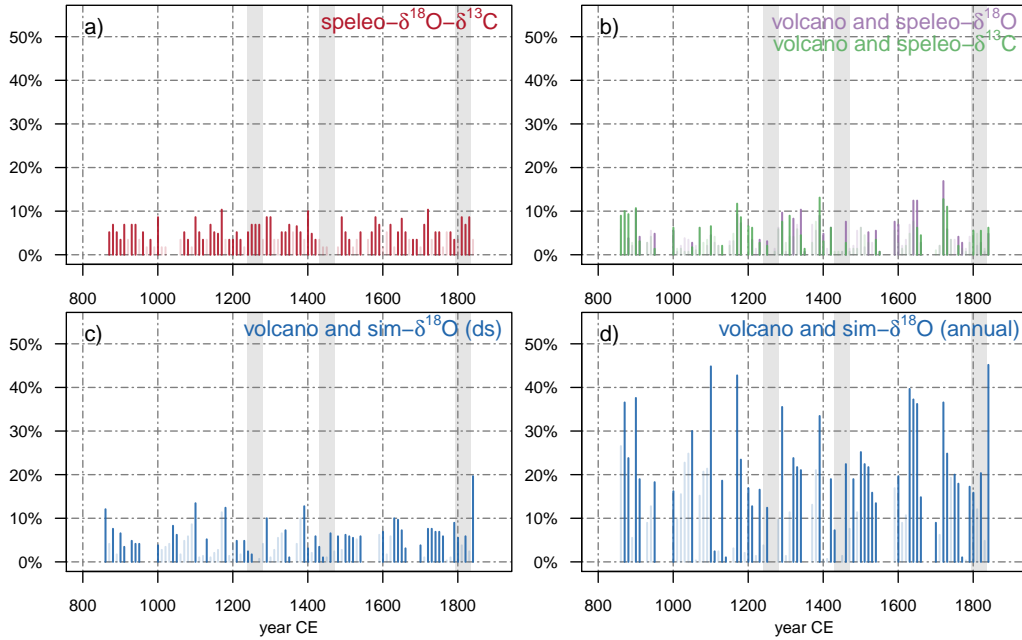
Figure 10. Synchronous events: a) the synchronous extreme events between $\delta^{18}O_{speleo}$ and $\delta^{13}C_{speleo}$ (red), b) the synchronous events between the speleothem isotopes (oxygen purple and carbon green), and volcanic eruptions as reconstructed by Crowley and Unterman (2013) or Gao et al. (2008) (depicted in Fig. 1d)), c) and d) the synchronous extreme events between simulated $\delta^{18}O$ values at the cave locations of all simulations in down-sampled to record resolution and annual resolution respectively. Where occurrence of synchronous extreme events is significant with $\alpha = 0.05$, the bars are shown in dark colors, non-significant in transparent colors. The four light grey bars in the background of each plot show areas of high volcanic activity.

5   To examine if there are factors that influence both $\delta^{18}O_{speleo}$ and $\delta^{13}C_{speleo}$ simultaneously, we analyze the similarity of both signals. 86 % of the speleothems show significant correlation between both isotopes (results not shown). A different test for similarity is provided by checking for synchronous extreme events in the time series.

    Fig. 10 shows the temporal distribution of extreme events globally. In Fig. 10a) we test for synchronous extreme events between the two isotopes by studying their relative timing to changes in volcanic forcing. Despite the high number of
10 significantly correlated oxygen and carbon isotopes within one record, global patterns are not visible with a maximum of

10% of speleothems showing synchronous extreme events between $\delta^{18}O_{speleo}$ and $\delta^{13}C_{speleo}$ at the same time over the last millennium. Synchronous events are also not higher in time periods of strong volcanic eruptions (indicated by grey bars).

By analyzing synchronous events between volcanic eruptions as reconstructed by Crowley and Unterman (2013) and Gao et al. (2008) (Fig. 1d) and $\delta^{18}O_{speleo}$ as in Fig. 10b), up to 20% of speleothems exhibit extreme events at the same time as extreme volcanic eruptions. This share is higher than for the carbon isotopes, where up to 15% exhibit extreme events synchronous to volcanic eruptions. Both isotopes also show pronounced peaks occurring with different extreme volcano events (indicated by grey background) but also for minor volcanic events.

To check if the speleothems used here can resolve global extreme events of short duration, we compare $\delta^{18}O_{iw}$ at the cave locations of each simulation to the volcanic forcing of the simulations (see Tab. 1). While up to 50% of $\delta^{18}O_{iw}$ at cave locations and annual resolution exhibit an extreme event at the same time as an extreme volcanic eruption (Fig. 10d), this number largely decreases to less than half when the resolution of $\delta^{18}O_{iw}$ is decreased to that of the speleothems (10c). The number of pseudo-speleothems experiencing synchronous events to volcanic forcing (Fig. 10c) is more similar to that of the speleothems (Fig. 10b). Summarizing, we see no global temporal pattern of synchronous extreme events in both $\delta^{18}O_{speleo}$ and $\delta^{13}C_{speleo}$ (Fig. 10a). A lower temporal resolution strongly decreases the ability of the modelled archive to resolve global events like volcanic eruptions.

5 Discussion

5.1 Comparison of oxygen isotope variability in isotope-enabled models and speleothems during the last millennium

We found that the mean $\delta^{18}O_{iw}$ fields show global differences of up to $2.12\,‰$ between the models, that could most likely be attributed to the global mean temperature differences of up to 1.8 K between the models. Similarly, most of the strong regional differences in $\delta^{18}O_{iw}$ between models could be explained by regional differences in simulated temperature (SFig. 5). This can be expected following the temperature effect (Dansgaard, 1964) or the more recently observed changes in isotopic signatures under the current anthropogenic warming trend (Rozanski et al., 1992). Temperature differences are, however, not the only explanation for differences in isotopic signatures between models, and individual model biases are also visible (SFig 1 and 2). Specifically, we found less depletion of $\delta^{18}O_{iw}$ in isoGSM over Antarctica as an artifact of its numerical scheme used for moisture transport, and linked to extremely dry regions (Yoshimura et al., 2008). The warm bias in high latitudes for ECHAM5-wiso results is known to underestimate isotopic depletion (Werner et al., 2011, 2016). Overestimation of fractionation processes in iCESM during re-evaporation processes resulted in generally stronger depletion in $\delta^{18}O_{sim}$ (Brady et al., 2019). The cool bias in northern mid-latitudes in the GISS-E2-R model as found in Schmidt et al. (2014) resulted in more depleted $\delta^{18}O_{iw}$ in this region. Colder temperatures over Antarctica in iHadCM3 explained partly why isotopic signatures are a lot more depleted than in the other simulations. The iHadCM3 data, however, compares well to historical ice core data (Tindall et al., 2009), suggesting that the colder Antarctic conditions modelled by iHadCM3 may be more consistent with reality than the multi-model mean. Even though this study mostly focused on a terrestrial mid-to-low latitude archive, local differences of modelled isotopic signatures in the Antarctic may have an influence on isotopic representation in the general circulation of the models.

At the cave locations, the spread between the simulations yielded $4.51\,‰$ (90% CI: 3.96, 4.79) in median (Fig. 3), while the median disagreement between simulated and speleothem $\delta^{18}O_{dweq}$ was around $-0.38\,‰$ $(-0.8, -0.23)$ (Fig. 4). This means that even though the simulations differed strongly in some regions, using multiple models can be sufficient to average out the disagreement at individual cave locations. The differences to the speleothems are in agreement with those found by Bühler et al. (2021) who compared the SISALv2 database to the iHadCM3 last millennium simulation. Median differences

to the speleothem records were small for all models, where differences spatially around the globe (Fig. 3) reflected both the internal variability of models, as well as global differences between the models. For example, ECHAM5-wiso showed the highest values for $\delta^{18}O_{iw}$ in the global mean and also a more positive distribution than the other models. Differences in global mean $\delta^{18}O_{iw}$ may arise from the weighting by the simulated evaporation and precipitation amounts, and while

5   evaporation in ECHAM5-wiso is similar to the other models (SFig. 6), precipitation amounts are lower (SFig. 7). The lower oceanic precipitation amout can most likely be attributed to the coarser vertical resolution of ECHAM5-wiso (Hagemann et al., 2006).

Our analysis suggests that a multi-model approach is advisable whenever comparing mean modelled values to measured data. Even though global mean $\delta^{18}O_{iw}$ values may be comparable, local and regional temperature estimates, and, therefore,

10   modelled $\delta^{18}O_{iw}$ values can vary strongly and deviate between models. Even though isoGSM displayed the lowest disagreement between $\delta^{18}O_{iw}$ and $\delta^{18}O_{speleo}$ (Fig. 4), additional processes between meteoric water above the cave and drip water may again influence this difference. The multi-model offset comparison justified the use of the multi-model mean at cave locations in the following spatial analysis.

We found significant relationships between all considered modelled climatic variables (temperature, precipitation, and

15   evaporation) and $\delta^{18}O_{iw}$, to mean $\delta^{18}O_{dweq}$ (Fig. 7). In general, the temperature and altitude effects on $\delta^{18}O_{speleo}$ are visible in all latitude bands. Effects such as the precipitation-amount relationship to $\delta^{18}O_{speleo}$, is more distinct in the tropical and subtropical latitude band, which is in line with the effects described by Dansgaard (1964). In the extratropics, the precipitation effect is weak and overlapped by the altitude effect. We restricted our analysis to temperature, precipitation, and evaporation as they were available for all models. Future analyses that include more model diagnostics across the multi-

20   model ensemble may find relationships to different variables that will improve our understanding on model biases and to obtain a coherent picture of which variables drive $\delta^{18}O$ in the model world. The relationships between speleothem mean $\delta^{13}C_c$ and meteorological variables from model ensemble mean (Fig. 8) were less clear, which again point to a more local influence.

Global studies that have evaluated $\delta^{18}O_{speleo}$ isotopic signatures using climate models already exist (Bühler et al., 2021;

25   Comas-Bru et al., 2019; Midhun et al., 2021), where regions with shared climatic features showed stronger relationships. For example, Baker et al. (2019) focused on specific climate zones by comparing drip-water measurements to precipitation $\delta^{18}O$ measurements and was able to identify temperature zones for which mean measured $\delta^{18}O$ or $\delta^{18}O_{iw}$ was most similar to $\delta^{18}O_{speleo}$. In our study, we found stronger relationships to climate variables in the individual latitude bands than on a global scale as in Bühler et al. (2021). Analyzing regions with high data density and similar climate patterns, we found even

30   stronger temperature relationships (SFig. 8 and SFig. 9). Still, local particularities, such as large elevation difference over short distances, could not be resolved properly by the simulations and explained many of the stronger outliers, especially in the tropics.

Comparing a last century subset of the SISALv1 database by Fohlmeister et al. (2020) with our last millennium SISALv2-subset yielded similar results for precipitation and altitude relationships to $\delta^{13}C_{speleo}$ (SFig. 10). In contrast to our latitudinal

35   approach, they compared $\delta^{13}C_{speleo}$ to temperature on a global scale. They neglected clusters of speleothems where factors other than temperature play an important role for the carbon isotope composition (e.g. high amounts of precipitation, known cave specific particularities and processes, or temperatures close to the natural limit of vegetation ($< 5°C$)). The remaining records with temperatures between ~ 7 to $27°C$ showed a positive trend between $\delta^{13}C_{speleo}$ and temperature. This trend is in contrast to our observation based on clustering the records according to latitudinal bands. With this approach, we find

40   no relationship between $\delta^{13}C_{speleo}$ and temperature for the tropics and subtropics, but a clear inverse relationship between modelled temperatures and $\delta^{13}C_{speleo}$ is observed for the extratropical records.

Higher cave site elevation coincided significantly with more depleted $\delta^{18}O_{dweq}$, which is in line with the altitude effect (Dansgaard, 1964). For $\delta^{13}C_{speleo}$, local studies exist that predict an increase in $\delta^{13}C_{speleo}$ with higher altitude (Johnston

et al., 2013). However, for the global last millennium subset of the SISALv2 database more entities with carbon measurements in higher altitudes are needed to see a potential global relationship, in addition to the relationship we find in the extratropical latitude bands.

5.2 Can models reproduce variability archived in speleothems?

5   For all simulations, temperature variability was the dominant driver in $\delta^{18}O_{iw}$ at high latitudes and precipitation variability at low latitudes and parts of the Antarctic (Fig. 5c and SFig. 5). However, local and regional climate dynamics, such as landward moisture transport and ice sheet changes can mask and alter these relationships, as found for simulated isotopes in GISS-E2-R in a global study by LeGrande and Schmidt (2009). At the cave sites, model-internal regional variability as well as the records' age uncertainties substantially decreased correlation estimates. We observed that the sign of the correlation

10   estimated between simulated temperature and $\delta^{18}O_{iw}$ agreed at 60% of cave locations for ≥ 3 simulations, and at 26% for ≥ 4 simulations. For correlation estimates to precipitation, this was true only at 11% or 1% of locations, respectively. When compared to measured $\delta^{18}O_{speleo}$, we found more significant temporal correlation estimates to modelled temperature than to modelled precipitation. This could in part be explained by global temperature responses to e.g. volcanic forcing being more uniform between model ensemble runs compared to precipitation responses, which depend strongly on regional

15   particularities. Regions with high inter-model climate variable spread (SFig. 11) also coincided with regions of the fewest significant correlation estimates to simulated temperature and the least agreement between the climatic drivers of $\delta^{18}O_{sim}$.

     For variability specifically at the cave site locations, $\delta^{13}C_{speleo}$ appeared to be more variable than $\delta^{18}O_{speleo}$ on average on all timescales (Fig 9d) with an increasingly higher variability compared to $\delta^{18}O_{speleo}$ towards centennial timescales and longer (Fig 9a). Within 86% of all speleothems where both isotopes are provided, $\delta^{18}O_{speleo}$ and $\delta^{13}C_{speleo}$ showed sig-

20   nificant correlations. Jointly explained variance in the isotopic signal can point towards common climatic drivers. However, the amplified variance on long timescales in $\delta^{13}C_{speleo}$ could either hint at changes in the water cycle but also in land surface processes such as soil formation or vegetation composition and density. Considering more terrestrial archives as well as trace elements stored within the speleothems may help to better disentangle the climatic and environmental signals. On decadal and shorter timescales, where the meteoric and seasonal vegetation isotopic signal is mostly smoothed by the karst

25   system, higher variability in $\delta^{13}C_{speleo}$ may result from the stronger isotopic fractionation for carbon compared to oxygen in precipitated calcite (Polag et al., 2010; Hansen et al., 2019).

     Climate models reflected $\delta^{18}O_{iw}$ variability at cave locations to different extents. A clear offset between the models could be found on all timescales. We found no relationship between spatial resolution of the model and the variability of isotopic composition of precipitation. The higher-resolution run of iCESM and the lower-resolution run of iHadCM3 seem to show

30   similar variability globally and the lower-resolution ECHAM5-wiso shows even higher variability at the cave locations. Due to the strong impact of temperature and precipitation on $\delta^{18}O_{sim}$ variability we expect that this difference in isotopic variability also stems from the difference in the simulated climate. Further assessments using multivariate statistics are needed to firmly attribute the impact of climate on recorded variability of $\delta^{18}O$.

     The lower temporal resolution of speleothem records largely explained the model-data mismatch on decadal and shorter

35   timescales. Slow growth rates and limited sampling resolution lead to averaging effects which in turn lead to lower variability on decadal and shorter timescales. Simple karst-filters of a realistic transit time of ~ 2.5 yr as in SFig. 12) (as used in Bühler et al., 2021; Midhun et al., 2021; Dee et al., 2015) showed that variations in models and speleothems on these shorter timescales are similar, if accounted for. Expert knowledge of the local cave hydrology is, however, needed for a more detailed assessment on which model reflects $\delta^{18}O_{iw}$ variability best on decadal and shorter time scales compared to speleothems and

40   may still be restricted by karst and cave internal processes that effectively limit the sampling of climatic signals.

On decadal and longer timescales models seemed to underestimate $\delta^{18}O_{speleo}$ variability, although to different extents, with isoGSM showing the highest variability and the smallest model-data mismatch. The model-data mismatch that we observed between speleothems and $\delta^{18}O_{iw}$ starting at decadal timescales is in agreement with previous studies as by Laepple and Huybers (2014b). However, it is worth mentioning that speleothems may also be capable of enhancing climate-driven changes of $\delta^{18}O$ and $\delta^{13}C$ by cave-specific processes, resulting in higher variability on decadal and longer timescales. Under the assumption that variability on decadal and longer timescales is recorded correctly by speleothems, the iCESM model showed the strongest variability mismatch and isoGSM the smallest.

Cave locations were not necessarily reflective of mean annual $\delta^{18}O$ variability globally - at least not in the model simulations. Simulations that showed generally high variability at cave locations at speleothem resolution also tended to be more variable globally and vice versa for low variability. However, simulations that were less variable at cave locations than others can still be more variable globally. In our case, this trend could likely be attributed to the bias of geographic locations of the cave sites as the models mostly show high variance in $\delta^{18}O_{iw}$ in very dry regions and around the regions influenced by the Intertropical Convergence Zone.

5.3 Can external forcings be resolved by speleothems?

We found that 86% of speleothems show a significant temporal correlation between speleothem oxygen and carbon isotopes, with 47% even showing strong significant (anti-) correlations of $|c| > 0.5$. High co-variability between both isotopes can either be caused by kinetic fractionation processes (Hendy, 1971) in the cave environment or may be externally forced. For example, (Fohlmeister et al., 2017) studied a stalagmite in an arid region and found strong correlation between the isotopes. They attribute increased correlation to times of strong variations in cave-internal processes triggered by variations of external conditions. This simultaneity agrees with our findings that generally no extreme event in isotopes precedes the other, which can, however, also be attributed to low sampling resolution. More local cave monitoring studies are necessary to potentially exclude kinetic fractionation effects as the dominant driver.

Temporal coherence between model and data can only be expected in the frequency space. Variability associated with external forcing such as volcanic eruptions or changes in solar forcing, may however be imprinted in both model and data in a congruent time history (PAGESHydro2k-Consortium, 2017). Changes in temperature or precipitation due to aerosol forced cooling have been analyzed in a $\delta^{13}C$ record as signs of volcanic signatures of speleothems (Ridley et al., 2015). Growth rate changes (Baker et al., 1995) or the measurement of trace elements such as sulphur (Frisia et al., 2008) are other techniques to detect volcanic signals in speleothems but they generally require up to sub-annual resolution records. In our global analysis of 58 $\delta^{13}C_{speleo}$ and 89 $\delta^{18}O_{speleo}$ records, we saw no significant increase in extreme events in the isotope records coinciding with major volcanic eruptions. The individual isotopes yielded more distinct signatures of volcanic eruptions with up to 20% (15%) of speleothems recording synchronous extreme events in $\delta^{18}O_{speleo}$ ($\delta^{13}C_{speleo}$) and a volcanic eruption, similar to $\delta^{18}O_{iw}$ at record resolution. Both stayed, however, well below the possible simulated detection at cave locations under annual resolution of up to 50%. The comparison to the synchronous events to the down-sampled $\delta^{18}O_{iw}$ showed that the ability to capture events such as volcanic eruptions strongly decreases with record resolution. The attribution of specific peaks in speleothem data to volcanic events needs caution because of age-uncertainties and other possible explanations for the changes e.g. human settlements close-by (Baker et al., 1995). Increasing the bin size to the average age-uncertainty within the last millennium sub-set of the SISALv2 yielded the same results (SFig. 13).

Solar variations are another external forcing which is often invoked as an influence on the monsoon cycle that has been investigated using speleothem records (Neff et al., 2001; Lone et al., 2014; Cosford et al., 2008). In these studies, it is also standard to use high-resolution speleothems with a lowest resolution of about 5 yr for Lone et al. (2014). We repeated the analysis for Fig. 10 to analyze synchronous extreme events of $\delta^{18}O_{speleo}$ and $\delta^{13}C_{speleo}$ to the total solar irradiance

input (SFig. 14). While the general effects of decreased detectability with decreased resolution are also visible, the overall detection of extreme solar irradiance was much weaker than for volcanic eruptions. This was not only true at cave locations but globally when comparing simulated surface climate variables to solar variations (results not shown). As solar variation on this timescale is mostly cyclical compared to random extreme volcanic eruptions (compare Fig. 1), these results were to be expected from the methods used and are not in contradiction to the literature.

The impact of different climatic backgrounds on the δ^{18}O signal in speleothem records or paleoclimate simulations in time periods such as the Last Glacial Maximum and the Holocene have been studied extensively (e.g. Comas-Bru et al., 2019; Tierney et al., 2020; Parker et al., 2021). Periods of documented warmer and colder periods within the last millennium are for example the Little Ice Age (1550-1850 CE) or the Medieval Climate Anomaly (850-1250CE) (definitions from Jones et al., 2001). We note that neither the global mean surface temperature, nor the simulated δ^{18}O or the global δ^{18}O as recorded by the speleothems, showed significant changes to the mean state on a global scale within the described periods within the last millennium (results not shown). This is in line with Neukom et al. (2019) who found no global coherence of cold or warm periods over the Common Era, even though local changes are observable (e.g. McDermott et al., 2001).

Summarizing, the comparison to modelled valued showed that cave locations in this study are in general suitable to detect δ^{18}O$_{iw}$ variations due to modelled climatic changes in response to changes in volcanic or solar forcing. Even though speleothems are highly resolved archives with small age-uncertainties compared to other archives, the median resolution during the last millennium of 6.08 yr (4.07, 7.85) was not enough to resolve changes in δ^{13}C$_{speleo}$ or δ^{18}O$_{speleo}$ due to potential solar or volcanically–induced climatic changes. Karst-mixing effects which dampen the signal, may decrease the ability to detect these changes even further.

5.4 Limitations

A current weakness of this type of analysis is that we only compared δ^{18}O$_{sim}$ of PMIP version 3 generation models to archived isotopes. However, parameter and tuning choices within one model, especially in the cloud and convection scheme, have a strong imprint on δ^{18}O$_{sim}$ signatures (for example Nusbaumer et al. (2017) for iCESM, Field et al. (2014) for GISS-E2-R). To further systematically explore and constrain modelled δ^{18}O, a multi-model ensemble under different model set-ups will be needed. The multi-model comparison in this study only included how different models represent the oxygen isotopes, as δ^{13}C is not included in isotope-enabled models yet. For iCESM, a carbon cycle in the ocean exists (Jahn et al., 2015) and great effort is put into the incorporation of a carbon-cycle to isotope-enabled GCMs by the scientific community. However, this incorporation into GCMs cannot resolve the cave carbon cycle. Proxy system models of intermediate complexity that explicitly model soil carbon isotopes processes, temperature, moisture and vegetation above the cave can be a more useful approach.

We also only looked at δ^{18}O and δ^{13}C as possible proxies for climatic changes. In contrast to e.g. ice-cores, speleothems do not directly record precipitation δ^{18}O. Instead, both δ^{18}O$_{speleo}$ and δ^{13}C$_{speleo}$ undergo fractionation processes which are influenced by various cave-internal processes which may not be climate related (Lachniet, 2009; Fairchild and Baker, 2012; Hartmann and Baker, 2017; Dreybrodt and Scholz, 2011). Considering additional processes such as prior calcite precipitation (PCP) or other geochemical climate-related proxies can help to decipher the climatic signal from karst- or cave-internal processes (Kaufmann, 2003; Schwarcz et al., 1976; Owen et al., 2016; Tremaine and Froelich, 2013; Noronha et al., 2014).

When comparing the speleothem isotopes to volcanic data, we note that there now are more recent volcanic reconstructions available, which suggest a modification to the timing or magnitude of last millennium eruptions (Sigl et al., 2015). Given the temporal resolution of the speleothems, changes in timing of volcanic events would impact the comparisons of model data to only those speleothems with high temporal resolution. As only the timing of the extreme event is compared, a change in

magnitude would be irrelevant. As for the comparison with the simulated data, only the response of the model to any given eruption is important (Colose et al., 2016b), as we did not compare the timing of extreme events in speleothems to those in the simulation.

5   Compared to the capability of speleothems to cover complete glacial-interglacial cycles, we instead looked at short timescales when focusing on the last millennium and what drives variability on decadal to centennial timescales. The last millennium is considered a relatively stable time period and climatic changes might not be strong enough to be fully captured by speleothems. On longer timescales, speleothems may still be a good archive to capture these larger changes (Genty et al., 2006).

6   Conclusion

10 We presented a multi-model comparison over five last millennium isotope-enabled simulations (ECHAM5-wiso, GISS-E2-R, iCESM, iHadCM3 and isoGSM) and compared their representation of isotopic signatures in mean and variability to paleoclimate data from a large speleothem database (a last millennium subset of SISALv2). We found that $\delta^{18}O_{iw}$ differed substantially between models on a regional scale as well as at speleothem cave sites. This could in part be attributed to differences in simulated temperature, model biases in implementing SWI or topography, but also cave- and site-specific

15 controls on speleothem isotopes. Extreme model values that differ greatly from the rest can be compensated for by using the multi-model mean and thus reducing local spatial biases. The isoGSM simulation showed the lowest absolute mean difference to the speleothems at cave locations, while all other simulations show only slightly higher disagreements. Variability on decadal and longer timescales in the speleothems was higher than indicated by models and was also best represented by isoGSM, which, however, still underestimated variability on these timescales. No relationship was found between the spatial

20 resolution of the models and their variability of the isotopic composition of precipitation. In all models, temperature was driving $\delta^{18}O_{iw}$ variability in high latitudes and precipitation in low latitudes. At cave site locations in particular, which are mostly located in low- to mid-latitudes, models agreed more on temperature being the driving factor of SWI variability than on precipitation.

    Dividing the global set into latitude bands, we were able to distinguish temperature and altitude relationships for both the

25 oxygen and the carbon isotopes, as well as significant relationships for $\delta^{18}O_{dweq}$ to other simulated climate variables. While most records showed significant correlation between the two isotopes, using both isotopes to gain more information than just from one remained difficult. Especially, variations in solar and volcanic forcing are not imprinted in either the single isotope or the pair on a global scale. Many archive limitations could, however, be attributed to the low resolution of the data-set compared to the processes expected to be resolved.

30   This joint intercomparison of stable water isotopologue variability in both models and speleothem data is the first dataset in a time period of natural forcing and allows for further future analysis by the scientific community. Our analysis encourages the use of multi-model means whenever possible as already suggested by other studies (Colose et al., 2016a). From the point of model evaluation, the incorporation of different archives with higher resolution (e.g. corals, trees, ice cores as in the Iso2k database (Konecky et al., 2020)) and with the help of improved proxy system models may provide further insight into why

35 offsets between models can be so large regionally. From a speleothem perspective, within-cave and between-cave variability comparisons using both isotopes will help to understand the recorded signal better and give higher confidence. Future multi-model comparisons of isotope-enabled models for other time periods are required to further evaluate biases in models, as well as comparisons to $\delta^{18}O$-archives of all kinds, to gain a deeper understanding of the underlying concept in what influences variability and co-variability of isotopes in speleothems.

Code and Data availability.

Code to reproduce figures and analyses will be made available in the final manuscript on GitHub. Model data as csv-files with output at cave locations (ECHAM5-wiso, GISS-E2-R, iCESM, iHadCM3, isoGSM) at annual and record resolution, as well as monthly fields of surface temperature, precipitation, isotopic composition of precipitation and evaporation or latent heat respectively for all simulations will be made freely available on Pangaea in the final manuscript. The SISAL (Speleothem Isotopes Synthesis and AnaLysis Working Group) database version 2 (SISALv2) is publicly available through the University of Reading repository at http://dx.doi.org/10.17864/1947.256 (Comas-Bru et al., 2020a). We use R for the data analysis (R Core Team, 2020a). The main packages are tidyverse (Wickham et al., 2019), ncdf4 (Pierce, 2019), ggplot2 (Wickham, 2016), raster (Hijmans, 2020), zoo (Zeileis and Grothendieck, 2005), plyr (Wickham, 2011), and (Wickham et al., 2021). We use the nest R package (https://github.com/krehfeld/nest Rehfeld et al., 2011; Rehfeld and Kurths, 2014) and the PaleoSpec package (https://github.com/EarthSystemDiagnostics/PaleoSpec, Kunz et al., 2020).

Author contributions. JB, JA, FL and KR designed this study. JB and JA wrote the paper and created the figures. FL and JF contributed with data interpretations. KR, JS, KY, MM, ALG and MW contributed with model data that JB and JA collected and standardized. JB prepared the speleothem data. JB, JA, KR, FS, JF, JS, KY, ALG, MM and MW contributed to the revisions of the manuscript. All authors approved of the final version of the paper.

Competing interests. The authors declare that they have no conflict of interest.

Acknowledgements. This study includes data compiled by SISAL (Speleothem Isotopes Synthesis and Analysis), a working group of the Past Global Changes (PAGES) project. PAGES received support from the Swiss Academy of Sciences and the Chinese Academy of Sciences. The project is in part inspired by discussions at the SISAL 4th workshop: Exploiting the SISALv2 database for evaluating climate processes, Xi'an, China, 14-18 October 2019. Nils Weitzel, Elisa Ziegler, Beatrice Ellerhoff, Qiong Zhang, Nikita Kaushal, Natasha Sekhon, Valdir Felipe Novello, Jon Baker, Ny Riavo Voarintsoa and Yuval Burstyn are acknowledged for helpful advice, comments and discussion on text and figures. Parts of the computations were enabled by resources provided by the Swedish National Infrastructure for Computing (SNIC) at the National Supercomputer Centre (NSC), partially funded by the Swedish Research Council through grant agreement no. 2018-05973.

Financial support. We acknowledge financial support from the Swedish Research Council (Vetenskapsrådet; grant nos. 2013-06476 and 2017-04232), the Deutsche Forschungsgemeinschaft (grant nos. 316076679 and 395588486), the Bundesministerium für Bildung und Forschung through the PalMod project (grant no. 01LP1926C), and the Swiss National Science Foundation (SNSF; grant no. P4P4P2_186693).

References

Amante, C. and Eakins, B. W.: ETOPO1 1 Arc-Minute Global Relief Model: Procedures, Data Sources and Analysis, https://doi.org/10.7289/V5C8276M, 2009.

Atsawawaranunt, K., Comas-Bru, L., Amirnezhad Mozhdehi, S., Deininger, M., Harrison, S. P., Baker, A., Boyd, M., Kaushal, N., Masood Ahmad, S., Ait Brahim, Y., Arienzo, M., Bajo, P., Braun, K., Burstyn, Y., Chawchai, S., Duan, W., Hatvani, I. G., Hu, J., Kern, Z., Labuhn, I., Lachniet, M., Lechleitner, F. A., Lorrey, A., Pérez-Mejías, C., Pickering, R., Scroxton, N., Atkinson, T., Ayalon, A., Baldini, J., Bar-Matthews, M., Bernal, J. P., Breitenbach, S., Boch, R., Borsato, A., Cai, Y., Carolin, S., Cheng, H., Columbu, A., Couchoid, I., Cruz, F., Demény, A., Dominguez-Villar, D., Drăgusin, V., Drysdale, R., Ersek, V., Finné, M., Fleitmann, D., Fohlmeister, J., Frappier, A., Genty, D., Holzkämper, S., Hopley, P., Kathayat, G., Keenan-Jones, D., Koltai, G., Luetscher, M., Li, T. Y., Lone, M. A., Markowska, M., Mattey, D., McDermott, F., Moreno, A., Moseley, G., Nehme, C., Novello, V. F., Psomiadis, D., Rehfeld, K., Ruan, J., Sekhon, N., Sha, L., Sholz, D., Shopov, Y., Smith, A., Strikis, N., Treble, P., Vaks, A., Vansteenberge, S., Veiga-Pires, C., Voarintsoa, N. R., Wang, X., Wong, C., Wortham, B., Wurtzel, J., and Zong, B.: The SISAL database: A global resource to document oxygen and carbon isotope records from speleothems, Earth System Science Data, 10, 1687–1713, https://doi.org/10.5194/essd-10-1687-2018, 2018.

Atwood, A., Wu, E., Frierson, D., Battisti, D., and Sachs, J.: Quantifying climate forcings and feedbacks over the last millennium in the CMIP5–PMIP3 models, Journal of Climate, 29, 1161–1178, 2016.

Baker, A., Smart, P. L., Barnes, W., Edwards, R. L., and Farrant, A.: The Hekla 3 volcanic eruption recorded in a Scottish speleothem?, The Holocene, 5, 336–342, 1995.

Baker, A., Bradley, C., Phipps, S. J., Fischer, M., Fairchild, I. J., Fuller, L., Spaptl, C., and Azcurra, C.: Millennial-length forward models and pseudoproxies of stalagmite δ18O: An example from NW Scotland, Climate of the Past, 8, 1153–1167, https://doi.org/10.5194/cp-8-1153-2012, 2012.

Baker, A., Hartmann, A., Duan, W., Hankin, S., Comas-Bru, L., Cuthbert, M. O., Treble, P. C., Banner, J., Genty, D., Baldini, L. M., Bartolomé, M., Moreno, A., Pérez-Mejías, C., and Werner, M.: Global analysis reveals climatic controls on the oxygen isotope composition of cave drip water, Nature Communications, 10, 2984, https://doi.org/10.1038/s41467-019-11027-w, 2019.

Baker, A. J., Mattey, D. P., and Baldini, J. U.: Reconstructing modern stalagmite growth from cave monitoring, local meteorology, and experimental measurements of dripwater films, Earth and Planetary Science Letters, 392, 239–249, https://doi.org/https://doi.org/10.1016/j.epsl.2014.02.036, 2014.

Baker, J. L., Lachniet, M. S., Chervyatsova, O., Asmerom, Y., and Polyak, V. J.: Holocene warming in western continental Eurasia driven by glacial retreat and greenhouse forcing, Nature Geoscience, 10, 430–435, https://doi.org/10.1038/ngeo2953, 2017.

Berger, A.: Long-term variations of daily insolation and Quaternary climatic changes, Journal of Atmospheric Sciences, 35, 2362–2367, 1978.

Berger, A. and Loutre, M.: Insolation values for the climate of the last 10 million years, Quaternary Science Reviews, 10, 297–317, https://doi.org/https://doi.org/10.1016/0277-3791(91)90033-Q, 1991.

Berkelhammer, M., Sinha, A., Stott, L., Cheng, H., Pausata, F. S. R., and Yoshimura, K.: An Abrupt Shift in the Indian Monsoon 4000 Years Ago, in: Geophysical Monograph Series, pp. 75–87, http://commons.wikimedia.org, 2012a.

Berkelhammer, M., Stott, L., Yoshimura, K., Johnson, K., and Sinha, A.: Synoptic and mesoscale controls on the isotopic composition of precipitation in the western United States, Climate Dynamics, 38, 433–454, https://doi.org/10.1007/s00382-011-1262-3, 2012b.

Bradley, R. S.: Paleoclimate: reconstructing climates of the Quaternary, Elsevier, 1999.

Brady, E., Stevenson, S., Bailey, D., Liu, Z., Noone, D., Nusbaumer, J., Otto-Bliesner, B. L., Tabor, C., Tomas, R., Wong, T., Zhang, J., and Zhu, J.: The Connected Isotopic Water Cycle in the Community Earth System Model Version 1, Journal of Advances in Modeling Earth Systems, 11, 2547–2566, https://doi.org/https://doi.org/10.1029/2019MS001663, 2019.

Breitenbach, S. F., Rehfeld, K., Goswami, B., Baldini, J. U., Ridley, H. E., Kennett, D. J., Prufer, K. M., Aquino, V. V., Asmerom, Y., Polyak, V. J., Cheng, H., Kurths, J., and Marwan, N.: Constructing proxy records from age models (COPRA), Climate of the Past, 8, 1765–1779, https://doi.org/10.5194/cp-8-1765-2012, 2012.

Bretagnon, P. and Francou, G.: Planetary theories in rectangular and spherical variables. VSOP 87 solutions, Astronomy and astrophysics, 202, 309–315, 1988.

Bühler, J. C., Roesch, C., Kirschner, M., Sime, L., Holloway, M. D., and Rehfeld, K.: Comparison of the oxygen isotope signatures in speleothem records and iHadCM3 model simulations for the last millennium, Climate of the Past Discussions, 2020, 1–30, https://doi.org/10.5194/cp-2020-121, 2020.

Bühler, J. C., Roesch, C., Kirschner, M., Sime, L., Holloway, M. D., and Rehfeld, K.: Comparison of the oxygen isotope signatures in speleothem records and iHadCM3 model simulations for the last millennium, Climate of the Past, 17, 985–1004, 2021.

Caplan, P., Derber, J., Gemmill, W., Hong, S. Y., Pan, H. L., and Parrish, D.: Changes to the 1995 NCEP operational medium-range forecast model analysis-forecast system, Weather and Forecasting, 12, 581–594, https://doi.org/10.1175/1520-0434(1997)012<0581:cttnom>2.0.co;2, 1997.

Chatfield, C.: The Analysis of Time Series - An Introduction, Chapman & Hall/CRC, sixth edition edn., 2003.

Cheng, H., Edwards, R. L., Sinha, A., Spötl, C., Yi, L., Chen, S., Kelly, M., Kathayat, G., Wang, X., Li, X., Kong, X., Wang, Y., Ning, Y., and Zhang, H.: The Asian monsoon over the past 640,000 years and ice age terminations, Nature, 534, 640–646, https://doi.org/10.1038/nature18591, https://www.nature.com/articles/nature18591, 2016.

Chiang, J. C., Herman, M. J., Yoshimura, K., and Fung, I. Y.: Enriched East Asian oxygen isotope of precipitation indicates reduced summer seasonality in regional climate and westerlies, Proceedings of the National Academy of Sciences of the United States of America, 117, 14 745–14 750, https://doi.org/10.1073/pnas.1922602117, 2020.

Colose, C. M., LeGrande, A. N., and Vuille, M.: The influence of volcanic eruptions on the climate of tropical South America during the last millennium in an isotope-enabled general circulation model, Climate of the Past, 12, 961–979, https://doi.org/10.5194/cp-12-961-2016, 2016a.

Colose, C. M., LeGrande, A. N., and Vuille, M.: Hemispherically asymmetric volcanic forcing of tropical hydroclimate during the last millennium, Earth System Dynamics, 7, 681–696, https://doi.org/10.5194/esd-7-681-2016, 2016b.

Comas-Bru, L., Harrison, S. P., Werner, M., Rehfeld, K., Scroxton, N., Veiga-Pires, C., and working group members, S.: Evaluating model outputs using integrated global speleothem records of climate change since the last glacial, Climate of the Past, 15, 1557–1579, https://doi.org/10.5194/cp-15-1557-2019, 2019.

Comas-Bru, L., Atsawawaranunt, K., Harrison, S., and working group members, S.: SISAL (Speleothem Isotopes Synthesis and AnaLysis Working Group) database version 2.0. University of Reading. Dataset, https://doi.org/10.17864/1947.256, 2020a.

Comas-Bru, L., Rehfeld, K., Roesch, C., Amirnezhad-Mozhdehi, S., Harrison, S. P., Atsawawaranunt, K., Ahmad, S. M., Brahim, Y. A., Baker, A., Bosomworth, M., Breitenbach, S. F. M., Burstyn, Y., Columbu, A., Deininger, M., Demény, A., Dixon, B., Fohlmeister, J., Hatvani, I. G., Hu, J., Kaushal, N., Kern, Z., Labuhn, I., Lechleitner, F. A., Lorrey, A., Martrat, B., Novello, V. F., Oster, J., Pérez-Mejías, C., Scholz, D., Scroxton, N., Sinha, N., Ward, B. M., Warken, S., Zhang, H., and members, S. W. G.: SISALv2: a comprehensive speleothem isotope database with multiple age–depth models, Earth System Science Data, 12, 2579–2606, https://doi.org/10.5194/essd-12-2579-2020, 2020b.

Conroy, J. L., Cobb, K. M., and Noone, D.: Comparison of precipitation isotope variability across the tropical Pacific in observations and SWING2 model simulations, Journal of Geophysical Research Atmospheres, 118, 5867–5892, https://doi.org/10.1002/jgrd.50412, 2013.

Coplen, T. B.: Reporting of stable carbon, hydrogen, and oxygen isotopic abundances, Tech. rep., International Atomic Energy Agency (IAEA), http://inis.iaea.org/search/search.aspx?orig_q=RN:27021329, 1995.

Coplen, T. B., Kendall, C., and Hopple, J.: Comparison of stable isotope reference samples, Nature, 302, 28–30, 1983.

Cosford, J., Qing, H., Eglington, B., Mattey, D., Yuan, D., Zhang, M., and Cheng, H.: East Asian monsoon variability since the Mid-Holocene recorded in a high-resolution, absolute-dated aragonite speleothem from eastern China, Earth and Planetary Science Letters, 275, 296–307, https://doi.org/https://doi.org/10.1016/j.epsl.2008.08.018, 2008.

Cox, P. M.: Description of the "TRIFFID" dynamic global vegetation model, Hadley Centre. Technical Note 24, p. 17, 2001.

Crowley, T. J. and Unterman, M. B.: Technical details concerning development of a 1200 yr proxy index for global volcanism, Earth System Science Data, 5, 187–197, https://doi.org/10.5194/essd-5-187-2013, 2013.

Crowley, T. J., Zielinski, G., Vinther, B., Udisti, R., Kreutz, K., Cole-Dai, J., and Castellano, E.: Volcanism and the Little Ice Age, PAGES news, 16, 22–23, https://doi.org/10.22498/pages.16.2.22, 2008.

Dalaiden, Q., Goosse, H., Klein, F., Lenaerts, J. T., Holloway, M., Sime, L., and Thomas, E. R.: How useful is snow accumulation in reconstructing surface air temperature in Antarctica? A study combining ice core records and climate models, Cryosphere, 14, 1187–1207, https://doi.org/10.5194/tc-14-1187-2020, 2020.

Dansgaard, W.: Stable isotopes in precipitation, Tellus, 16, 436–468, https://doi.org/10.3402/tellusa.v16i4.8993, 1964.

Dee, S., Emile-Geay, J., Evans, M. N., Allam, A., Steig, E. J., and Thompson, D.: PRYSM: An open-source framework for PRoxY System Modeling, with applications to oxygen-isotope systems, Journal of Advances in Modeling Earth Systems, 7, 1220–1247, https://doi.org/https://doi.org/10.1002/2015MS000447, 2015.

Dolman, A., Kunz, T., Groeneveld, J., and Laepple, T.: Estimating the timescale-dependent uncertainty of paleoclimate records—a spectral approach. Part II: Application and interpretation, Climate of The Past Discussions, pp. 1–38, https://doi.org/10.5194/cp-2019-153, 2020.

Dreybrodt, W. and Scholz, D.: Climatic dependence of stable carbon and oxygen isotope signals recorded in speleothems: From soil water to speleothem calcite, Geochimica et Cosmochimica Acta, 75, 734–752, https://doi.org/https://doi.org/10.1016/j.gca.2010.11.002, 2011.

Duan, W., Ruan, J., Luo, W., Li, T., Tian, L., Zeng, G., Zhang, D., Bai, Y., Li, J., Tao, T., et al.: The transfer of seasonal isotopic variability between precipitation and drip water at eight caves in the monsoon regions of China, Geochimica et Cosmochimica Acta, 183, 250–266, 2016.

Eyring, V., Bony, S., Meehl, G. A., Senior, C. A., Stevens, B., Stouffer, R. J., and Taylor, K. E.: Overview of the Coupled Model Intercomparison Project Phase 6 (CMIP6) experimental design and organization, Geoscientific Model Development, 9, 1937–1958, https://doi.org/10.5194/gmd-9-1937-2016, 2016.

Fairchild, I. J. and Baker, A.: Speleothem science: from process to past environments, John Wiles & Sons, 2012.

Field, R. D., Kim, D., LeGrande, A. N., Worden, J., Kelley, M., and Schmidt, G. A.: Evaluating climate model performance in the tropics with retrievals of water isotopic composition from Aura TES, Geophysical Research Letters, 41, 6030–6036, https://doi.org/https://doi.org/10.1002/2014GL060572, 2014.

Fleitmann, D., Burns, S. J., Mangini, A., Mudelsee, M., Kramers, J., Villa, I., Neff, U., Al-Subbary, A. A., Buettner, A., Hippler, D., and Matter, A.: Holocene ITCZ and Indian monsoon dynamics recorded in stalagmites from Oman and Yemen (Socotra), Quaternary Science Reviews, 26, 170–188, https://doi.org/https://doi.org/10.1016/j.quascirev.2006.04.012, 2007.

Fohlmeister, J., Schröder-Ritzrau, A., Scholz, D., Spötl, C., Riechelmann, D. F. C., Mudelsee, M., Wackerbarth, A., Gerdes, A., Riechelmann, S., Immenhauser, A., Richter, D. K., and Mangini, A.: Bunker Cave stalagmites: an archive for central European Holocene climate variability, Climate of the Past, 8, 1751–1764, https://doi.org/10.5194/cp-8-1751-2012, 2012.

Fohlmeister, J., Plessen, B., Dudashvili, A. S., Tjallingii, R., Wolff, C., Gafurov, A., and Cheng, H.: Winter precipitation changes during the Medieval Climate Anomaly and the Little Ice Age in arid Central Asia, Quaternary Science Reviews, 178, 24–36, https://doi.org/https://doi.org/10.1016/j.quascirev.2017.10.026, 2017.

Fohlmeister, J., Arps, J., Spötl, C., Schröder-Ritzrau, A., Plessen, B., Günter, C., Frank, N., and Trüssel, M.: Carbon and oxygen isotope fractionation in the water-calcite-aragonite system, Geochimica et Cosmochimica Acta, 235, 127–139, https://doi.org/https://doi.org/10.1016/j.gca.2018.05.022, 2018.

Fohlmeister, J., Voarintsoa, N. R. G., Lechleitner, F. A., Boyd, M., Brandstätter, S., Jacobson, M. J., and Oster, J. L.: Main controls on the stable carbon isotope composition of speleothems, Geochimica et Cosmochimica Acta, 279, 67–87, 2020.

Frisia, S., Borsato, A., and Susini, J.: Synchrotron radiation applications to past volcanism archived in speleothems: An overview, Journal of Volcanology and Geothermal Research, 177, 96–100, https://doi.org/https://doi.org/10.1016/j.jvolgeores.2007.11.010, explosive volcanism in the central Mediterranean area during the late Quaternary - linking sources and distal archives, 2008.

Gao, C., Robock, A., and Ammann, C.: Volcanic forcing of climate over the past 1500 years: An improved ice core-based index for climate models, Journal of Geophysical Research: Atmospheres, 113, https://doi.org/https://doi.org/10.1029/2008JD010239, 2008.

Genty, D., Blamart, D., Ghaleb, B., Plagnes, V., Causse, C., Bakalowicz, M., Zouari, K., Chkir, N., Hellstrom, J., Wainer, K., and Bourges, F.: Timing and dynamics of the last deglaciation from European and North African d13C stalagmite profiles—comparison with Chinese and South Hemisphere stalagmites, Quaternary Science Reviews, 25, 2118–2142, https://doi.org/https://doi.org/10.1016/j.quascirev.2006.01.030, 2006.

Gesch, D. B., Verdin, K. L., and Greenlee, S. K.: New land surface digital elevation model covers the Earth, Eos, Transactions American Geophysical Union, 80, 69–70, https://doi.org/10.5066/F7DF6PQS, 1999.

Gordon, C., Cooper, C., Senior, C. A., Banks, H. T., Gregory, J. M., Johns, T. C., Mitchell, J. F. B., and Wood, R. A.: The simulation of SST, sea ice extents and ocean heat transports in a version of the Hadley Centre coupled model without flux adjustments, Climate Dynamics, 16, 147–168, https://doi.org/https://doi.org/10.1007/s003820050010, 2000.

Goursaud, S., Masson-Delmotte, V., Favier, V., Orsi, A., and Werner, M.: Water stable isotope spatiooral variability in Antarctica in 1960-2013: Observations and simulations from the ECHAM5-wiso atmospheric general circulation model, Climate of the Past, 14, 923–946, https://doi.org/10.5194/cp-14-923-2018, 2018.

Grossman, E. L. and Ku, T. L.: Oxygen and carbon isotope fractionation in biogenic aragonite: Temperature effects, Chemical Geology: Isotope Geoscience Section, https://doi.org/10.1016/0168-9622(86)90057-6, 1986.

Guðlaugsdóttir, H., Steen-Larsen, H. C., Sjolte, J., Masson-Delmotte, V., Werner, M., and Sveinbjörnsdóttir, E.: The influence of volcanic eruptions on weather regimes over the North Atlantic simulated by ECHAM5/MPI-OM ensemble runs from 800 to 2000 CE, Atmospheric Research, 213, 211–223, https://doi.org/10.1016/j.atmosres.2018.04.021, 2018.

Guðlaugsdóttir, H., Sjolte, J., Sveinbjörnsdóttir, Á. E., Werner, M., and Steen-Larsen, H. C.: North Atlantic weather regimes in δ18O of winter precipitation: isotopic fingerprint of the response in the atmospheric circulation after volcanic eruptions, Tellus, Series B: Chemical and Physical Meteorology, 71, 1–19, https://doi.org/10.1080/16000889.2019.1633848, 2019.

Haese, B., Werner, M., and Lohmann, G.: Stable water isotopes in the coupled atmosphere-land surface model ECHAM5-JSBACH, Geoscientific Model Development, 6, 1463–1480, https://doi.org/10.5194/gmd-6-1463-2013, 2013.

Hagemann, S., Arpe, K., and Roeckner, E.: Evaluation of the hydrological cycle in the ECHAM5 model, Journal of Climate, 19, 3810–3827, https://doi.org/10.1175/JCLI3831.1, 2006.

Hansen, M., Scholz, D., Schöne, B. R., and Spötl, C.: Simulating speleothem growth in the laboratory: Determination of the stable isotope fractionation (d13C and d18O) between H2O, DIC and CaCO3, Chemical Geology, 509, 20–44, https://doi.org/https://doi.org/10.1016/j.chemgeo.2018.12.012, https://www.sciencedirect.com/science/article/pii/S0009254118305977, 2019.

Hartmann, A. and Baker, A.: Modelling karst vadose zone hydrology and its relevance for paleoclimate reconstruction, Earth-Science Reviews, 172, 178–192, https://doi.org/10.1016/j.earscirev.2017.08.001, 2017.

Hébert, R., Rehfeld, K., and Laepple, T.: Comparing estimation techniques for timescale-dependent scaling of climate variability in paleoclimate time series, Nonlinear Processes in Geophysics Discussions, 2021, 1–26, https://doi.org/10.5194/npg-2021-7, 2021.

Hendy, C.: The isotopic geochemistry of speleothems—I. The calculation of the effects of different modes of formation on the isotopic composition of speleothems and their applicability as palaeoclimatic indicators, Geochimica et Cosmochimica Acta, 35, 801–824, https://doi.org/https://doi.org/10.1016/0016-7037(71)90127-X, 1971.

Hijmans, R. J.: raster: Geographic Data Analysis and Modeling, https://CRAN.R-project.org/package=raster, r package version 3.0-12, 2020.

Holden, J., ed.: An introduction to physical geography and the environment, Pearson Education, 3 edn., 2012.

Holloway, M. D., Sime, L. C., Singarayer, J. S., Tindall, J. C., and Valdes, P. J.: Simulating the 128-ka Antarctic Climate Response to Northern Hemisphere Ice Sheet Melting Using the Isotope-Enabled HadCM3, Geophysical Research Letters, 45, 11,911–921,929, https://doi.org/10.1029/2018GL079647, 2018.

Hurrell, J. W., Holland, M. M., Gent, P. R., Ghan, S., Kay, J. E., Kushner, P. J., Lamarque, J.-F., Large, W. G., Lawrence, D., Lindsay, K., et al.: The community earth system model: a framework for collaborative research, Bulletin of the American Meteorological Society, 94, 1339–1360, 2013.

Hurtt, G. C., Chini, L. P., Frolking, S., Betts, R., Feddema, J., Fischer, G., Fisk, J., Hibbard, K., Houghton, R., Janetos, A., et al.: Harmonization of land-use scenarios for the period 1500–2100: 600 years of global gridded annual land-use transitions, wood harvest, and resulting secondary lands, Climatic change, 109, 117–161, 2011.

IPCC: Climate Change 2013: The Physical Science Basis. Contribution of Working Group I to the Fifth Assessment Report of the Intergovernmental Panel on Climate Change, Cambridge University Press, https://doi.org/10.1017/CBO9781107415324, 2013.

Jahn, A., Lindsay, K., Giraud, X., Gruber, N., Otto-Bliesner, B. L., Liu, Z., and Brady, E. C.: Carbon isotopes in the ocean model of the Community Earth System Model (CESM1), Geoscientific Model Development, 8, 2419–2434, https://doi.org/10.5194/gmd-8-2419-2015, 2015.

Jean-Baptiste, P., Genty, D., Fourré, E., and Régnier, E.: Tritium dating of dripwater from Villars Cave (SW-France), Applied Geochemistry, 107, 152–158, https://doi.org/10.1016/j.apgeochem.2019.06.005, 2019.

Johnston, V. E., Borsato, A., Spötl, C., Frisia, S., and Miorandi, R.: Stable isotopes in caves over altitudinal gradients: fractionation behaviour and inferences for speleothem sensitivity to climate change, Climate of the Past, 9, 99–118, https://doi.org/10.5194/cp-9-99-2013, 2013.

Jones, P. D., Osborn, T. J., and Briffa, K. R.: The Evolution of Climate Over the Last Millennium, Science, 292, 662–667, https://doi.org/10.1126/science.1059126, 2001.

Jungclaus, J. H., Keenlyside, N., Botzet, M., Haak, H., Luo, J. J., Latif, M., Marotzke, J., Mikolajewicz, U., and Roeckner, E.: Ocean circulation and tropical variability in the coupled model ECHAM5/MPI-OM, Journal of Climate, 19, 3952–3972, https://doi.org/10.1175/JCLI3827.1, 2006.

Jungclaus, J. H., Lorenz, S. J., Timmreck, C., Reick, C. H., Brovkin, V., Six, K., Segschneider, J., Giorgetta, M. A., Crowley, T. J., Pongratz, J., Krivova, N. A., Vieira, L. E., Solanki, S. K., Klocke, D., Botzet, M., Esch, M., Gayler, V., Haak, H., Raddatz, T. J., Roeckner, E., Schnur, R., Widmann, H., Claussen, M., Stevens, B., and Marotzke, J.: Climate and carbon-cycle variability over the last millennium, Climate of the Past, 6, 723–737, https://doi.org/10.5194/cp-6-723-2010, 2010.

Jungclaus, J. H., Bard, E., Baroni, M., Braconnot, P., Cao, J., Chini, L. P., Egorova, T., Evans, M., Fidel González-Rouco, J., Goosse, H., Hurtt, G. C., Joos, F., Kaplan, J. O., Khodri, M., Klein Goldewijk, K., Krivova, N., Legrande, A. N., Lorenz, S. J., Luterbacher, J., Man, W., Maycock, A. C., Meinshausen, M., Moberg, A., Muscheler, R., Nehrbass-Ahles, C., Otto-Bliesner, B. I., Phipps, S. J., Pongratz, J., Rozanov, E., Schmidt, G. A., Schmidt, H., Schmutz, W., Schurer, A., Shapiro, A. I., Sigl, M., Smerdon, J. E., Solanki, S. K., Timmreck, C., Toohey, M., Usoskin, I. G., Wagner, S., Wu, C. J., Leng Yeo, K., Zanchettin, D., Zhang, Q., and Zorita, E.: The PMIP4 contribution to CMIP6 - Part 3: The last millennium, scientific objective, and experimental design for the PMIP4 past1000 simulations, Geoscientific Model Development, 10, 4005–4033, https://doi.org/10.5194/gmd-10-4005-2017, 2017.

Kageyama, M., Braconnot, P., Harrison, S. P., Haywood, A. M., Jungclaus, J. H., Otto-Bliesner, B. L., Peterschmitt, J.-Y., Abe-Ouchi, A., Albani, S., Bartlein, P. J., Brierley, C., Crucifix, M., Dolan, A., Fernandez-Donado, L., Fischer, H., Hopcroft, P. O., Ivanovic, R. F., Lambert, F., Lunt, D. J., Mahowald, N. M., Peltier, W. R., Phipps, S. J., Roche, D. M., Schmidt, G. A., Tarasov, L., Valdes, P. J., Zhang, Q., and Zhou, T.: The PMIP4 contribution to CMIP6 – Part 1: Overview and over-arching analysis plan, Geoscientific Model Development, 11, 1033–1057, https://doi.org/10.5194/gmd-11-1033-2018, 2018.

Kanamitsu, M., Ebisuzaki, W., Woollen, J., Yang, S. K., Hnilo, J. J., Fiorino, M., and Potter, G. L.: NCEP-DOE AMIP-II reanalysis (R-2), Bulletin of the American Meteorological Society, 83, 1631–1644, https://doi.org/10.1175/bams-83-11-1631, 2002.

Kanner, L. C., Burns, S. J., Cheng, H., Edwards, R. L., and Vuille, M.: High-resolution variability of the South American summer monsoon over the last seven millennia: insights from a speleothem record from the central Peruvian Andes, Quaternary Science Reviews, 75, 1–10, https://doi.org/https://doi.org/10.1016/j.quascirev.2013.05.008, 2013.

Kathayat, G., Sinha, A., Tanoue, M., Yoshimura, K., Li, H., Zhang, H., and Cheng, H.: Interannual oxygen isotope variability in Indian summer monsoon precipitation reflects changes in moisture sources, Communications Earth & Environment, 2, 1–10, https://doi.org/10.1038/s43247-021-00165-z, 2021.

Kaufmann, G.: Stalagmite growth and palaeo-climate: the numerical perspective, Earth and Planetary Science Letters, 214, 251–266, https://doi.org/https://doi.org/10.1016/S0012-821X(03)00369-8, 2003.

Kendall, C. and Caldwell, E. A.: Chapter 2 - Fundamentals of Isotope Geochemistry, in: Fundamentals of Isotope Geochemistry, pp. 51–86, Elsevier, Amsterdam, https://doi.org/10.1016/B978-0-444-81546-0.50009-4, 1998.

Kennett, D. J., Breitenbach, S. F. M., Aquino, V. V., Asmerom, Y., Awe, J., Baldini, J. U., Bartlein, P., Culleton, B. J., Ebert, C., Jazwa, C., Macri, M. J., Marwan, N., Polyak, V., Prufer, K. M., Ridley, H. E., Sodemann, H., Winterhalder, B., and Haug, G. H.: Development and Disintegration of Maya Political Systems in Response to Climate Change, Science, 338, 788–791, https://doi.org/10.1126/science.1226299, 2012.

Konecky, B. L., McKay, N. P., Churakova (Sidorova), O. V., Comas-Bru, L., Dassié, E. P., DeLong, K. L., Falster, G. M., Fischer, M. J., Jones, M. D., Jonkers, L., Kaufman, D. S., Leduc, G., Managave, S. R., Martrat, B., Opel, T., Orsi, A. J., Partin, J. W., Sayani, H. R., Thomas, E. K., Thompson, D. M., Tyler, J. J., Abram, N. J., Atwood, A. R., Cartapanis, O., Conroy, J. L., Curran, M. A., Dee, S. G., Deininger, M., Divine, D. V., Kern, Z., Porter, T. J., Stevenson, S. L., von Gunten, L., and Members, I. P.: The Iso2k database: a global compilation of paleo-δ^{18}O and δ^2H records to aid understanding of Common Era climate, Earth System Science Data, 12, 2261–2288, https://doi.org/10.5194/essd-12-2261-2020, 2020.

Kunz, T., Dolman, A. M., and Laepple, T.: Estimating the timescale-dependent uncertainty of paleoclimate records – a spectral approach. Part I: Theoretical concept, Climate of the Past Discussions, 2020, 1–38, https://doi.org/10.5194/cp-2019-150, 2020.

Lachniet, M. S.: Climatic and environmental controls on speleothem oxygen-isotope values, Quaternary Science Reviews, 28, 412–432, https://doi.org/10.1016/j.quascirev.2008.10.021, 2009.

Laepple, T. and Huybers, P.: Global and regional variability in marine surface temperatures, Geophysical Research Letters, 41, 2528–2534, https://doi.org/10.1002/2014GL059345, 2014a.

Laepple, T. and Huybers, P.: Ocean surface temperature variability: Large model–data differences at decadal and longer periods, Proceedings of the National Academy of Sciences, 111, 16 682–16 687, https://doi.org/10.1073/pnas.1412077111, 2014b.

Landrum, L., Otto-Bliesner, B. L., Wahl, E. R., Conley, A., Lawrence, P. J., Rosenbloom, N., and Teng, H.: Last millennium climate and its variability in CCSM4, Journal of Climate, 26, 1085–1111, https://doi.org/10.1175/JCLI-D-11-00326.1, 2013.

Langebroek, P. M., Werner, M., and Lohmann, G.: Climate information imprinted in oxygen-isotopic composition of precipitation in Europe, Earth and Planetary Science Letters, 311, 144–154, https://doi.org/10.1016/j.epsl.2011.08.049, 2011.

Latombe, G., Burke, A., Vrac, M., Levavasseur, G., Dumas, C., Kageyama, M., and Ramstein, G.: Comparison of spatial downscaling methods of general circulation model results to study climate variability during the Last Glacial Maximum, Geoscientific Model Development, 11, 2563–2579, https://doi.org/10.5194/gmd-11-2563-2018, https://gmd.copernicus.org/articles/11/2563/2018/, 2018.

Lean, J.: Calculations of Solar Irradiance: monthly means from 1882 to 2008, annual means from 1610 to 2008, pp. 1–4, https://doi.org/10.1007/s00159-004, 2009.

Lechleitner, F. A., Day, C. C., Kost, O., Wilhelm, M., Haghipour, N., Henderson, G. M., and Stoll, H. M.: Stalagmite carbon isotopes suggest deglacial increase in soil respiration in western Europe driven by temperature change, Climate of the Past, 17, 1903–1918, https://doi.org/10.5194/cp-17-1903-2021, https://cp.copernicus.org/articles/17/1903/2021/, 2021.

Legrande, A. N. and Anchukaitis, K. J.: Volcanic eruptions and climate, PAGES Magazine, 23, 2015.

LeGrande, A. N. and Schmidt, G. A.: Sources of Holocene variability of oxygen isotopes in paleoclimate archives, Climate of the Past, 5, 441–455, https://doi.org/10.5194/cp-5-441-2009, 2009.

Lewis, S. C. and Legrande, A. N.: Stability of ENSO and its tropical Pacific teleconnections over the Last Millennium, Climate of the Past, 11, 1347–1360, https://doi.org/10.5194/cp-11-1347-2015, 2015.

Lone, M. A., Ahmad, S. M., Dung, N. C., Shen, C.-C., Raza, W., and Kumar, A.: Speleothem based 1000-year high resolution record of Indian monsoon variability during the last deglaciation, Palaeogeography, Palaeoclimatology, Palaeoecology, 395, 1–8, https://doi.org/https://doi.org/10.1016/j.palaeo.2013.12.010, 2014.

Lundeen, Z., Brunelle, A., Burns, S. J., Polyak, V., and Asmerom, Y.: A speleothem record of Holocene paleoclimate from the northern Wasatch Mountains, southeast Idaho, USA, Quaternary International, 310, 83–95, https://doi.org/https://doi.org/10.1016/j.quaint.2013.03.018, pACLIM: Proceedings of the 25th Pacific Climate Workshop, 2011, 2013.

MacFarling Meure, C., Etheridge, D., Trudinger, C., Steele, P., Langenfelds, R., Van Ommen, T., Smith, A., and Elkins, J.: Law Dome CO2, CH4 and N2O ice core records extended to 2000 years BP, Geophysical Research Letters, 33, https://doi.org/10.1029/2006GL026152, 2006.

Marland, G., Boden, T. A., and Andres, R. J.: Global, Regional, and National Fossil Fuel CO2 Emissions. In Trends: A Compendium of Data on Global Change, Tech. rep., Carbon Dioxide Information Analysis Center, Oak Ridge National Laboratory, U.S. Department of Energy, Oak Ridge, Tenn., U.S.A., 2003.

Marsland, S. J., Haak, H., Jungclaus, J. H., Latif, M., and Röske, F.: The Max-Planck-Institute global ocean/sea ice model with orthogonal curvilinear coordinates, Ocean Modelling, 5, 91–127, https://doi.org/10.1016/S1463-5003(02)00015-X, 2002.

MATLAB: Version 9.5.0.944444 (R2018b), The MathWorks Inc., Natick, Massachusetts, 2018.

McDermott, F., Mattey, D. P., and Hawkesworth, C.: Centennial-scale holocene climate variability revealed by a high-resolution speleothem δ18O record from SW Ireland, Science, 294, 1328–1331, https://doi.org/10.1126/science.1063678, 2001.

Medina-Elizalde, M., Burns, S. J., Polanco-Martínez, J. M., Beach, T., Lases-Hernández, F., Shen, C.-C., and Wang, H.-C.: High-resolution speleothem record of precipitation from the Yucatan Peninsula spanning the Maya Preclassic Period, Global and Planetary Change, 138,

93–102, https://doi.org/https://doi.org/10.1016/j.gloplacha.2015.10.003, climate Change and Archaeology in Mesoamerica: A Mirror for the Anthropocene, 2016.

Midhun, M. and Ramesh, R.: Validation of δ18O as a proxy for past monsoon rain by multi-GCM simulations, Climate Dynamics, 46, 1371–1385, https://doi.org/10.1007/s00382-015-2652-8, 2016.

5 Midhun, M., Stevenson, S., and Cole, J.: Oxygen isotopic signatures of major climate modes and implications for detectability in speleothems, Geophysical Research Letters, 48, e2020GL089 515, 2021.

Miller, R. L., Schmidt, G. A., Nazarenko, L. S., Tausnev, N., Bauer, S. E., Delgenio, A. D., Kelley, M., Lo, K. K., Ruedy, R., Shindell, D. T., Aleinov, I., Bauer, M., Bleck, R., Canuto, V., Chen, Y., Cheng, Y., Clune, T. L., Faluvegi, G., Hansen, J. E., Healy, R. J., Kiang, N. Y., Koch, D., Lacis, A. A., Legrande, A. N., Lerner, J., Menon, S., Oinas, V., Pérez García-Pando, C., Perlwitz, J. P., Puma,

10 M. J., Rind, D., Romanou, A., Russell, G. L., Sato, M., Sun, S., Tsigaridis, K., Unger, N., Voulgarakis, A., Yao, M. S., and Zhang, J.: CMIP5 historical simulations (1850-2012) with GISS ModelE2, Journal of Advances in Modeling Earth Systems, 6, 441–477, https://doi.org/10.1002/2013MS000266, 2014.

Morice, C. P., Kennedy, J. J., Rayner, N. A., and Jones, P. D.: Quantifying uncertainties in global and regional temperature change using an ensemble of observational estimates: The HadCRUT4 data set, Journal of Geophysical Research Atmospheres, 117, 1–22,

15 https://doi.org/10.1029/2011JD017187, 2012.

Muscheler, R., Joos, F., Beer, J., Müller, S. A., Vonmoos, M., and Snowball, I.: Solar activity during the last 1000 yr inferred from radionuclide records, Quaternary Science Reviews, 26, 82–97, https://doi.org/10.1016/j.quascirev.2006.07.012, 2007.

Muscheler, R., Adolphi, F., Herbst, K., and Nilsson, A.: The Revised Sunspot Record in Comparison to Cosmogenic Radionuclide-Based Solar Activity Reconstructions, Solar Physics, 291, 3025–3043, https://doi.org/10.1007/s11207-016-0969-z, 2016.

20 National Geophysical Data Center: 5-minute Gridded Global Relief Data (ETOPO5), https://doi.org/10.7289/V5D798BF, 1993.

Neale, R. B., Chen, C.-C., Gettelman, A., Lauritzen, P. H., Park, S., Williamson, D. L., Conley, A. J., Garcia, R., Kinnison, D., Lamarque, J.-F., et al.: Description of the NCAR community atmosphere model (CAM 5.0), NCAR Tech. Note NCAR/TN-486+ STR, 1, 1–12, 2010.

Neff, U., Burns, S. J., Mangini, A., Mudelsee, M., Fleitmann, D., and Matter, A.: Strong coherence between solar variability and the

25 monsoon in Oman between 9 and 6 kyr ago, Nature, 411, 290–293, https://doi.org/10.1038/35077048, 2001.

Neukom, R., Steiger, N., Gómez-Navarro, J. J., Wang, J., and Werner, J. P.: No evidence for globally coherent warm and cold periods over the preindustrial Common Era, Nature, 571, 550–554, https://doi.org/10.1038/s41586-019-1401-2, 2019.

NOAA National Geophysical Data Center: ETOPO1 1 Arc-Minute Global Relief Model, 2009.

Noronha, A. L., Johnson, K. R., Hu, C., Ruan, J., Southon, J. R., and Ferguson, J. E.: Assessing influences on speleothem dead carbon

30 variability over the Holocene: Implications for speleothem-based radiocarbon calibration, Earth and Planetary Science Letters, 394, 20–29, https://doi.org/https://doi.org/10.1016/j.epsl.2014.03.015, https://www.sciencedirect.com/science/article/pii/S0012821X14001599, 2014.

Novello, V., Cruz, F., Karmann, I., Burns, S., Stríkis, N., Vuille, M., Cheng, H., Lawrence Edwards, R., Santos, R., Frigo, E., and Barreto, E.: Multidecadal climate variability in Brazil's Nordeste during the last 3000 years based on speleothem isotope records, Geophysical

35 Research Letters, 39, https://doi.org/10.1029/2012GL053936, 2012.

Novello, V. F., Cruz, F. W., McGlue, M. M., Wong, C. I., Ward, B. M., Vuille, M., Santos, R. A., Jaqueto, P., Pessenda, L. C., Atorre, T., Ribeiro, L. M., Karmann, I., Barreto, E. S., Cheng, H., Edwards, R. L., Paula, M. S., and Scholz, D.: Vegetation and environmental changes in tropical South America from the last glacial to the Holocene documented by multiple cave sediment proxies, Earth and Planetary Science Letters, 524, 115 717, https://doi.org/https://doi.org/10.1016/j.epsl.2019.115717, 2019.

40 Novello, V. F., William da Cruz, F., Vuille, M., Pereira Silveira Campos, J. L., Stríkis, N. M., Apaéstegui, J., Moquet, J. S., Azevedo, V., Ampuero, A., Utida, G., Wang, X., Paula-Santos, G. M., Jaqueto, P., Ruiz Pessenda, L. C., Breecker, D. O., and Karmann, I.: Investigating d13C values in stalagmites from tropical South America for the last two millennia, Quaternary Science Reviews, 255, 106 822, https://doi.org/https://doi.org/10.1016/j.quascirev.2021.106822, 2021.

Nusbaumer, J., Wong, T. E., Bardeen, C., and Noone, D.: Evaluating hydrological processes in the Community Atmosphere

45 Model Version 5 (CAM5) using stable isotope ratios of water, Journal of Advances in Modeling Earth Systems, 9, 949–977, https://doi.org/https://doi.org/10.1002/2016MS000839, 2017.

Oleson, K. W., Bonan, G. B., Feddema, J., Vertenstein, M., and Kluzek, E.: Technical description of an urban parameterization for the Community Land Model (CLMU), NCAR, Boulder, 10, D6K35RM9, 2010.

Otto-Bliesner, B. L., Brady, E. C., Fasullo, J., Jahn, A., Landrum, L., Stevenson, S., Rosenbloom, N., Mai, A., and Strand, G.: Climate variability and change since 850 CE: An ensemble approach with the Community Earth System Model, Bulletin of the American Meteorological Society, 97, 735–754, 2016.

Owen, R., Day, C., Hu, C.-Y., Liu, Y.-H., Pointing, M., Blättler, C., and Henderson, G.: Calcium isotopes in caves as a proxy for aridity: Modern calibration and application to the 8.2 kyr event, Earth and Planetary Science Letters, 443, 129–138, https://doi.org/https://doi.org/10.1016/j.epsl.2016.03.027, https://www.sciencedirect.com/science/article/pii/S0012821X16301145, 2016.

PAGES2k-Consortium: Consistent multidecadal variability in global temperature reconstructions and simulations over the Common Era, Nature Geoscience, 12, 643–649, https://doi.org/10.1038/s41561-019-0400-0, 2019.

PAGESHydro2k-Consortium: Comparing proxy and model estimates of hydroclimate variability and change over the Common Era, Climate of the Past, 13, 1851–1900, https://doi.org/10.5194/cp-13-1851-2017, 2017.

Pardaens, A. K., Banks, H. T., Gregory, J. M., and Rowntree, P. R.: Freshwater transports in HadCM3, Climate Dynamics, 21, 177–195, https://doi.org/10.1007/s00382-003-0324-6, 2003.

Parker, S. E., Harrison, S. P., Comas-Bru, L., Kaushal, N., LeGrande, A. N., and Werner, M.: A data–model approach to interpreting speleothem oxygen isotope records from monsoon regions, Climate of the Past, 17, 1119–1138, https://doi.org/10.5194/cp-17-1119-2021, 2021.

Paul, J., Fortuin, F., and Kélder, H.: An ozone climatology based on ozonesonde and satellite measurements, Journal of Geophysical Research Atmospheres, 103, 31 709–31 734, https://doi.org/10.1029/1998jd200008, 1998.

Phipps, S. J., Mcgregor, H. V., Gergis, J., Gallant, A. J., Neukom, R., Stevenson, S., Ackerley, D., Brown, J. R., Fischer, M. J., and Van Ommen, T. D.: Paleoclimate data-model comparison and the role of climate forcings over the past 1500 years, Journal of Climate, 26, 6915–6936, https://doi.org/10.1175/JCLI-D-12-00108.1, https://journals.ametsoc.org/view/journals/clim/26/18/jcli-d-12-00108.1.xml, 2013.

Pierce, D.: ncdf4: Interface to Unidata netCDF (Version 4 or Earlier) Format Data Files, https://CRAN.R-project.org/package=ncdf4, r package version 1.17, 2019.

Polag, D., Scholz, D., Mühlinghaus, C., Spötl, C., Schröder-Ritzrau, A., Segl, M., and Mangini, A.: Stable isotope fractionation in speleothems: Laboratory experiments, Chemical Geology, 279, 31–39, https://doi.org/https://doi.org/10.1016/j.chemgeo.2010.09.016, https://www.sciencedirect.com/science/article/pii/S0009254110003414, 2010.

Pongratz, J., Reick, C., Raddatz, T., and Claussen, M.: A reconstruction of global agricultural areas and land cover for the last millennium, Global Biogeochemical Cycles, 22, https://doi.org/10.1029/2007GB003153, 2008.

Pope, V. D., Gallani, M. L., Rowntree, P. R., and Stratton, R. A.: The impact of new physical parametrizations in the Hadley Centre climate model: HadAM3, Climate Dynamics, 16, 123–146, https://doi.org/10.1007/s003820050009, 2000.

R Core Team: R: A Language and Environment for Statistical Computing, R Foundation for Statistical Computing, Vienna, Austria, https://www.R-project.org/, 2020a.

R Core Team: R: A Language and Environment for Statistical Computing, R Foundation for Statistical Computing, Vienna, Austria, https://www.R-project.org/, 2020b.

Rehfeld, K. and Kurths, J.: Similarity estimators for irregular and age-uncertain time series, Climate of the Past, pp. 107–122, https://doi.org/10.5194/cp-10-107-2014, 2014.

Rehfeld, K., Marwan, N., Heitzig, J., and Kurths, J.: Comparison of correlation analysis techniques for irregularly sampled time series, Nonlinear Processes in Geophysics, pp. 389–404, https://doi.org/10.5194/npg-18-389-2011, 2011.

Rehfeld, K., Münch, T., Ho, S. L., and Laepple, T.: Golbal paterns of declining temperature variability from the Last Glacial Maximum to the Holocene, Nature, 554, 356–359, https://doi.org/10.1038/nature25454, 2018.

Ridley, H. E., Asmerom, Y., Baldini, J. U., Breitenbach, S. F., Aquino, V. V., Prufer, K. M., Culleton, B. J., Polyak, V., Lechleitner, F. A., Kennett, D. J., et al.: Aerosol forcing of the position of the intertropical convergence zone since AD 1550, Nature Geoscience, 8, 195–200, 2015.

Risi, C., Noone, D., Worden, J., Frankenberg, C., Stiller, G., Kiefer, M., Funke, B., Walker, K., Bernath, P., Schneider, M., Wunch, D., Sherlock, V., Deutscher, N., Griffith, D., Wennberg, P. O., Strong, K., Smale, D., Mahieu, E., Barthlott, S., Hase, F., García, O., Notholt, J., Warneke, T., Toon, G., Sayres, D., Bony, S., Lee, J., Brown, D., Uemura, R., and Sturm, C.: Process-evaluation of tropospheric humidity simulated by general circulation models using water vapor isotopologues: 1. Comparison between models and observations, Journal of Geophysical Research Atmospheres, 117, n/a–n/a, https://doi.org/10.1029/2011JD016621, 2012.

Roeckner, E., Bäuml, G., Bonaventura, L., Brokopf, R., Esch, M., Giorgetta, M., Hagemann, S., Kirchner, I., Kornblueh, L., Manzini, E., Rhodin, A., Schlese, U., Schulzweida, U., and Tompkins, A.: The Atmospheric General Circulation Model ECHAM5. Part I: Model description, Tech. rep., Max Planck Institute for Meteorology, Hamburg, Germany, 2003.

Romanek, C. S., Grossman, E. L., and Morse, J. W.: Carbon isotopic fractionation in synthetic aragonite and calcite: Effects of temperature and precipitation rate, Geochimica et Cosmochimica Acta, 56, 419–430, https://doi.org/https://doi.org/10.1016/0016-7037(92)90142-6, 1992.

Rozanski, K., Araguãs-Araguãs, L., and Gonfiantini, R.: Relation between long-term trends of oxygen-18 isotope composition of precipitation and climate, Science, 258, 981–985, https://doi.org/10.1126/science.258.5084.981, 1992.

Schmidt, G. A., Hoffmann, G., Shindell, D. T., and Hu, Y.: Modeling atmospheric stable water isotopes and the potential for constraining cloud processes and stratosphere-troposphere water exchange, Journal of Geophysical Research Atmospheres, 110, 1–15, https://doi.org/10.1029/2005JD005790, 2005.

Schmidt, G. A., Ruedy, R., Hansen, J. E., Aleinov, I., Bell, N., Bauer, M., Bauer, S., Cairns, B., Canuto, V., Cheng, Y., Del Genio, A., Faluvegi, G., Friend, A. D., Hall, T. M., Hu, Y., Kelley, M., Kiang, N. Y., Koch, D., Lacis, A. A., Lerner, J., Lo, K. K., Miller, R. L., Nazarenko, L., Oinas, V., Perlwitz, J., Perlwitz, J., Rind, D., Romanou, A., Russell, G. L., Sato, M., Shindell, D. T., Stone, P. H., Sun, S., Tausnev, N., Thresher, D., and Yao, M. S.: Present-day atmospheric simulations using GISS ModelE: Comparison to in situ, satellite, and reanalysis data, Journal of Climate, 19, 153–192, https://doi.org/10.1175/JCLI3612.1, 2006.

Schmidt, G. A., Jungclaus, J. H., Ammann, C. M., Bard, E., Braconnot, P., Crowley, T. J., Delaygue, G., Joos, F., Krivova, N. A., Muscheler, R., Otto-Bliesner, B. L., Pongratz, J., Shindell, D. T., Solanki, S. K., Steinhilber, F., and Vieira, L. E. A.: Climate forcing reconstructions for use in PMIP simulations of the last millennium (v1.0), Geoscientific Model Development, 4, 33–45, https://doi.org/10.5194/gmd-4-33-2011, 2011.

Schmidt, G. A., Jungclaus, J. H., Ammann, C. M., Bard, E., Braconnot, P., Crowley, T. J., Delaygue, G., Joos, F., Krivova, N. A., Muscheler, R., Otto-Bliesner, B. L., Pongratz, J., Shindell, D. T., Solanki, S. K., Steinhilber, F., and Vieira, L. E. A.: Climate forcing reconstructions for use in PMIP simulations of the Last Millennium (v1.1), Geoscientific Model Development, 5, 185–191, https://doi.org/10.5194/gmd-5-185-2012, 2012.

Schmidt, G. A., Kelley, M., Nazarenko, L., Ruedy, R., Russell, G. L., Aleinov, I., Bauer, M., Bauer, S. E., Bhat, M. K., Bleck, R., Canuto, V., Chen, Y. H., Cheng, Y., Clune, T. L., Del Genio, A., De Fainchtein, R., Faluvegi, G., Hansen, J. E., Healy, R. J., Kiang, N. Y., Koch, D., Lacis, A. A., Legrande, A. N., Lerner, J., Lo, K. K., Matthews, E. E., Menon, S., Miller, R. L., Oinas, V., Oloso, A. O., Perlwitz, J. P., Puma, M. J., Putman, W. M., Rind, D., Romanou, A., Sato, M., Shindell, D. T., Sun, S., Syed, R. A., Tausnev, N., Tsigaridis, K., Unger, N., Voulgarakis, A., Yao, M. S., and Zhang, J.: Configuration and assessment of the GISS ModelE2 contributions to the CMIP5 archive, Journal of Advances in Modeling Earth Systems, 6, 141–184, https://doi.org/10.1002/2013MS000265, 2014.

Scholz, D., Frisia, S., Borsato, A., Spötl, C., Fohlmeister, J., Mudelsee, M., Miorandi, R., and Mangini, A.: Holocene climate variability in north-eastern Italy: potential influence of the NAO and solar activity recorded by speleothem data, Climate of the Past, 8, 1367–1383, https://doi.org/10.5194/cp-8-1367-2012, 2012.

Schurer, A. P., Tett, S. F. B., and Hegerl, G. C.: Small influence of solar variability on climate over the past millennium, Nature Geoscience, 7, 104–108, https://doi.org/10.1038/ngeo2040, 2014.

Schwarcz, H. P., Harmon, R. S., Thompson, P., and Ford, D. C.: Stable isotope studies of fluid inclusions in speleothems and their paleoclimatic significance, Geochimica et Cosmochimica Acta, 40, 657–665, https://doi.org/https://doi.org/10.1016/0016-7037(76)90111-3, 1976.

Shukla, P., Skea, J., Calvo Buendia, E., Masson-Delmotte, V., Pörtner, H., Roberts, D., Zhai, P., Slade, R., Connors, S., Van Diemen, R., et al.: IPCC, 2019: Climate Change and Land: an IPCC special report on climate change, desertification, land degradation, sustainable land management, food security, and greenhouse gas fluxes in terrestrial ecosystems, 2019.

Sigl, M., Winstrup, M., McConnell, J. R., Welten, K. C., Plunkett, G., Ludlow, F., Büntgen, U., Caffee, M., Chellman, N., Dahl-Jensen, D., et al.: Timing and climate forcing of volcanic eruptions for the past 2,500 years, Nature, 523, 543–549, 2015.

Sime, L. C., Tindall, J. C., Wolff, E. W., Connolley, W. M., and Valdes, P. J.: Antarctic isotopic thermometer during a CO2 forced warming event, Journal of Geophysical Research Atmospheres, 113, 1–16, https://doi.org/10.1029/2008JD010395, 2008.

5 Sime, L. C., Kohfeld, K. E., Le Quéré, C., Wolff, E. W., de Boer, A. M., Graham, R. M., and Bopp, L.: Southern Hemisphere westerly wind changes during the Last Glacial Maximum: Model-data comparison, Quaternary Science Reviews, https://doi.org/10.1016/j.quascirev.2012.12.008, 2013.

Sjolte, J., Sturm, C., Adolphi, F., Vinther, B. M., Werner, M., Lohmann, G., and Muscheler, R.: Solar and volcanic forcing of North Atlantic climate inferred from a process-based reconstruction, Climate of the Past, 14, 1179–1194, https://doi.org/10.5194/cp-14-1179-2018, 2018.

10 Steinhilber, F., Beer, J., and Fröhlich, C.: Total solar irradiance during the Holocene, Geophysical Research Letters, 36, 1–5, https://doi.org/10.1029/2009GL040142, 2009.

Stevenson, S., Otto-Bliesner, B. L., Brady, E. C., Nusbaumer, J., Tabor, C., Tomas, R., Noone, D. C., and Liu, Z.: Volcanic Eruption Signatures in the Isotope-Enabled Last Millennium Ensemble, Paleoceanography and Paleoclimatology, 34, 1534–1552, https://doi.org/10.1029/2019PA003625, 2019.

15 Sturm, C., Zhang, Q., and Noone, D.: An introduction to stable water isotopes in climate models: Benefits of forward proxy modelling for paleoclimatology, Climate of the Past, 6, 115–129, https://doi.org/10.5194/cp-6-115-2010, 2010.

Sun, Z., Yang, Y., Zhao, J., Tian, N., and Feng, X.: Potential ENSO effects on the oxygen isotope composition of modern speleothems: Observations from Jiguan Cave, central China, Journal of Hydrology, 566, 164–174, https://doi.org/https://doi.org/10.1016/j.jhydrol.2018.09.015, 2018.

20 Tan, L., Cai, Y., An, Z., Edwards, R. L., Cheng, H., Shen, C.-C., and Zhang, H.: Centennial- to decadal-scale monsoon precipitation variability in the semi-humid region, northern China during the last 1860 years: Records from stalagmites in Huangye Cave, The Holocene, 21, 287–296, https://doi.org/10.1177/0959683610378880, 2011.

Taylor, K. E., Stouffer, R. J., and Meehl, G. A.: An overview of CMIP5 and the experiment design, Bulletin of the American meteorological Society, 93, 485–498, 2012.

25 Tierney, J. E., Zhu, J., King, J., Malevich, S. B., Hakim, G. J., and Poulsen, C. J.: Glacial cooling and climate sensitivity revisited, Nature, 584, 569–573, 2020.

Tindall, J., Flecker, R., Valdes, P., Schmidt, D. N., Markwick, P., and Harris, J.: Modelling the oxygen isotope distribution of ancient seawater using a coupled ocean-atmosphere GCM: Implications for reconstructing early Eocene climate, Earth and Planetary Science Letters, https://doi.org/10.1016/j.epsl.2009.12.049, 2010.

30 Tindall, J. C., Valdes, P. J., and Sime, L. C.: Stable water isotopes in HadCM3: Isotopic signature of El Niño-Southern Oscillation and the tropical amount effect, Journal of Geophysical Research Atmospheres, 114, 1–12, https://doi.org/10.1029/2008JD010825, 2009.

Treble, P. C., Fairchild, I. J., Griffiths, A., Baker, A., Meredith, K. T., Wood, A., and McGuire, E.: Impacts of cave air ventilation and in-cave prior calcite precipitation on Golgotha Cave dripwater chemistry, southwest Australia, Quaternary Science Reviews, 127, 61–72, https://doi.org/https://doi.org/10.1016/j.quascirev.2015.06.001, novel approaches to and new insights from speleothem-based climate reconstructions, 2015.

35 Tremaine, D. M. and Froelich, P. N.: Speleothem trace element signatures: A hydrologic geochemical study of modern cave dripwaters and farmed calcite, Geochimica et Cosmochimica Acta, 121, 522–545, https://doi.org/https://doi.org/10.1016/j.gca.2013.07.026, https://www.sciencedirect.com/science/article/pii/S0016703713004067, 2013.

40 Tremaine, D. M., Froelich, P. N., and Wang, Y.: Speleothem calcite farmed in situ: Modern calibration of δ18O and δ13C paleoclimate proxies in a continuously-monitored natural cave system, Geochimica et Cosmochimica Acta, https://doi.org/10.1016/j.gca.2011.06.005, 2011.

Valdes, P. J., Armstrong, E., Badger, M. P. S., Bradshaw, C. D., Bragg, F., Crucifix, M., Davies-Barnard, T., Day, J., Farnsworth, A., Gordon, C., Hopcroft, P. O., Kennedy, A. T., Lord, N. S., Lunt, D. J., Marzocchi, A., Parry, L. M., Pope, V., Roberts, W. H. G., Stone, E. J., Tourte, G. J. L., and Williams, J. H. T.: The BRIDGE HadCM3 family of climate models: HadCM3@Bristol v1.0, Geoscientific Model Development, 10, 3715–3743, https://doi.org/10.5194/gmd-10-3715-2017, 2017.

Van Rampelbergh, M., Fleitmann, D., Verheyden, S., Cheng, H., Edwards, L., De Geest, P., De Vleeschouwer, D., Burns, S. J., Matter, A., Claeys, P., and Keppens, E.: Mid- to late Holocene Indian Ocean Monsoon variability recorded in four speleothems from Socotra Island, Yemen, Quaternary Science Reviews, 65, 129–142, https://doi.org/https://doi.org/10.1016/j.quascirev.2013.01.016, 2013.

Vieira, L. E. A., Solanki, S. K., Krivova, N. A., and Usoskin, I.: Evolution of the solar irradiance during the Holocene, A&A, 531, A6, https://doi.org/10.1051/0004-6361/201015843, 2011.

Voarintsoa, N. R. G., Wang, L., Railsback, L. B., Brook, G. A., Liang, F., Cheng, H., and Edwards, R. L.: Multiple proxy analyses of a U/Th-dated stalagmite to reconstruct paleoenvironmental changes in northwestern Madagascar between 370CE and 1300CE, Palaeo-geography, Palaeoclimatology, Palaeoecology, 469, 138–155, https://doi.org/https://doi.org/10.1016/j.palaeo.2017.01.003, 2017.

Wackerbarth, A., Scholz, D., Fohlmeister, J., and Mangini, A.: Modelling the delta 18 O value of cave drip water and speleothem calcite, Earth and Planetary Science Letters, 299, 387–397, https://doi.org/10.1016/j.epsl.2010.09.019, 2010.

Wang, J. K., Johnson, K. R., Borsato, A., Amaya, D. J., Griffiths, M. L., Henderson, G. M., Frisia, S., and Mason, A.: Hy-droclimatic variability in Southeast Asia over the past two millennia, Earth and Planetary Science Letters, 525, 115 737, https://doi.org/https://doi.org/10.1016/j.epsl.2019.115737, 2019.

Wang, Y., Lean, J. L., and Sheeley, Jr., N. R.: Modeling the Sun's Magnetic Field and Irradiance since 1713, The Astrophysical Journal, 625, 522–538, https://doi.org/10.1086/429689, 2005.

Warken, S. F., Fohlmeister, J., Schröder-Ritzrau, A., Constantin, S., Spötl, C., Gerdes, A., Esper, J., Frank, N., Arps, J., Terente, M., Riechelmann, D. F., Mangini, A., and Scholz, D.: Reconstruction of late Holocene autumn/winter precipitation variability in SW Romania from a high-resolution speleothem trace element record, Earth and Planetary Science Letters, 499, 122–133, https://doi.org/https://doi.org/10.1016/j.epsl.2018.07.027, 2018.

Warken, S. F., Schorndorf, N., Stinnesbeck, W., Hennhoefer, D., Stinnesbeck, S. R., Förstel, J., Steidle, S. D., Avilés Olguin, J., and Frank, N.: Solar forcing of early Holocene droughts on the Yucatán peninsula, Scientific Reports, 11, 13 885, https://doi.org/10.1038/s41598-021-93417-z, 2021.

Werner, M.: Modelling stable water isotopes: Status and perspectives, EPJ Web of Conferences, 9, 73–82, https://doi.org/10.1051/epjconf/201009005, 2010.

Werner, M., Langebroek, P. M., Carlsen, T., Herold, M., and Lohmann, G.: Stable water isotopes in the ECHAM5 general circu-lation model: Toward high-resolution isotope modeling on a global scale, Journal of Geophysical Research Atmospheres, 116, https://doi.org/10.1029/2011JD015681, 2011.

Werner, M., Haese, B., Xu, X., Zhang, X., Butzin, M., and Lohmann, G.: Glacial-interglacial changes in H218O, HDO and deu-terium excess-results from the fully coupled ECHAM5/MPI-OM Earth system model, Geoscientific Model Development, 9, 647–670, https://doi.org/10.5194/gmd-9-647-2016, 2016.

Wickham, H.: The Split-Apply-Combine Strategy for Data Analysis, Journal of Statistical Software, 40, 1–29, http://www.jstatsoft.org/v40/i01/, 2011.

Wickham, H.: ggplot2: Elegant Graphics for Data Analysis, Springer-Verlag New York, https://ggplot2.tidyverse.org, 2016.

Wickham, H., Averick, M., Bryan, J., Chang, W., McGowan, L. D., François, R., Grolemund, G., Hayes, A., Henry, L., Hester, J., Kuhn, M., Pedersen, T. L., Miller, E., Bache, S. M., Müller, K., Ooms, J., Robinson, D., Seidel, D. P., Spinu, V., Takahashi, K., Vaughan, D., Wilke, C., Woo, K., and Yutani, H.: Welcome to the tidyverse, Journal of Open Source Software, 4, 1686, https://doi.org/10.21105/joss.01686, 2019.

Wickham, H., François, R., Henry, L., and Müller, K.: dplyr: A Grammar of Data Manipulation, https://CRAN.R-project.org/package=dplyr, r package version 1.0.7, 2021.

Williams, P. W. and Ford, D. C.: Global distribution of carbonate rocks, Zeitschrift für Geomorphologie Supplementband, 147, 1, 2006.

Wong, C. I. and Breecker, D. O.: Advancements in the use of speleothems as climate archives, Quaternary Science Reviews, 127, 1–18, https://doi.org/10.1016/j.quascirev.2015.07.019, 2015.

Xi, X.: A Review of Water Isotopes in Atmospheric General Circulation Models: Recent Advances and Future Prospects, International Journal of Atmospheric Sciences, 2014, 1–16, https://doi.org/10.1155/2014/250920, 2014.

Yoshimura, K., Kanamitsu, M., Noone, D., and Oki, T.: Historical isotope simulation using Reanalysis atmospheric data, Journal of Geophysical Research Atmospheres, 113, D19 108, https://doi.org/10.1029/2008JD010074, 2008.

Zeileis, A. and Grothendieck, G.: zoo: S3 Infrastructure for Regular and Irregular Time Series, Journal of Statistical Software, 14, 1–27, https://doi.org/10.18637/jss.v014.i06, 2005.

Zhang, J., Liu, Z., Brady, E. C., Oppo, D. W., Clark, P. U., Jahn, A., Marcott, S. A., and Lindsay, K.: Asynchronous warming and d18O evolution of deep Atlantic water masses during the last deglaciation, Proceedings of the National Academy of Sciences, 114, 11 075–11 080, https://doi.org/10.1073/pnas.1704512114, 2017.

Zhang, X., Sun, Z., Guan, H., Zhang, X., Wu, H., and Huang, Y.: GCM simulations of stable isotopes in the water cycle in comparison with GNIP observations over east asia, Acta Meteorologica Sinica, 26, 420–437, https://doi.org/10.1007/s13351-012-0403-x, 2012.

Zhu, J., Liu, Z., Brady, E., Otto-Bliesner, B., Zhang, J., Noone, D., Tomas, R., Nusbaumer, J., Wong, T., Jahn, A., and Tabor, C.: Reduced ENSO variability at the LGM revealed by an isotope-enabled Earth system model, Geophysical Research Letters, 44, 6984–6992, https://doi.org/https://doi.org/10.1002/2017GL073406, 2017.